7

Restricted displacements and diffraction phenomena

In 1978, Hayward, Tomlinson, and Packer [1] carried out a PGSE NMR experiment on water flowing at low Reynold's number through a pipe. Under Poiseuille flow, the probability distribution of velocities in the pipe is uniform, so that the averaged propagator for displacements is a hat function, as shown in Fig. 2.8. The corresponding echo attenuation, the Fourier spectrum of this propagator, therefore has the oscillatory character of a 'sinc' function. This pioneering experiment demonstrated for the first time that PGSE NMR echo-attenuation behaviour could encompass more than a superposition of Gaussians, and indeed could include manifestations of phase coherence arising from the spin displacement distribution.

Of course, laminar flow implies intrinsic correlations in molecular displacement. By contrast, self-diffusion is, by conventional wisdom, characterised by entirely uncorrelated molecular motion. From such a standpoint, one would not expect to observe coherence phenomena in the attenuation expression for a PGSE NMR measurement on diffusing molecules. Nonetheless, in 1991, observation of such coherence is precisely what was seen [2]. Using a molecular ensemble in which diffusion provided the only means of spin transport, this experiment revealed oscillatory echo-attenuation functions highly reminiscent of diffraction patterns. The crucial factor governing phase coherence in the spin system was the presence of reflecting walls. Remarkably, it was restricted diffusion that lay behind the effect. Despite the fact that the echo resulted from spin-bearing molecules diffusing under locally Gaussian displacement distributions, the boundary collisions were found to imprint in $E(g, \Delta)$, a spatio-spectral structure factor relating to the pore geometry, thus resulting in an intimate relationship between structure and dynamics. With this insight came recognition of earlier conjecture [3] that the PGSE NMR was akin to a scattering experiment in which the scattering wavevector q was determined by the time integral of the gradient pulse. So began the field of research known as 'diffusive diffraction' or 'q-space imaging'.

The 1991 diffraction pattern is shown in Fig. 7.1.[1] This pattern results from a PGSE NMR experiment carried out on water diffusing in a porous matrix comprising close-packed polymer spheres of diameter $\sim$ 16 microns. As the diffusive observation

[1]Note that we consistently use the angular frequency representation of q, whereas a more direct correspondence with inverse structural features results from the use of the cyclic spatial frequency, $\check{q} = q/2\pi$. Consequently 'diffractograms' are generally plotted in terms of $\check{q}$, a practice followed here.

Translational Dynamics and Magnetic Resonance, First Edition, Paul T. Callaghan, © Paul T. Callaghan 2011.
Published in 2011 by Oxford University Press.

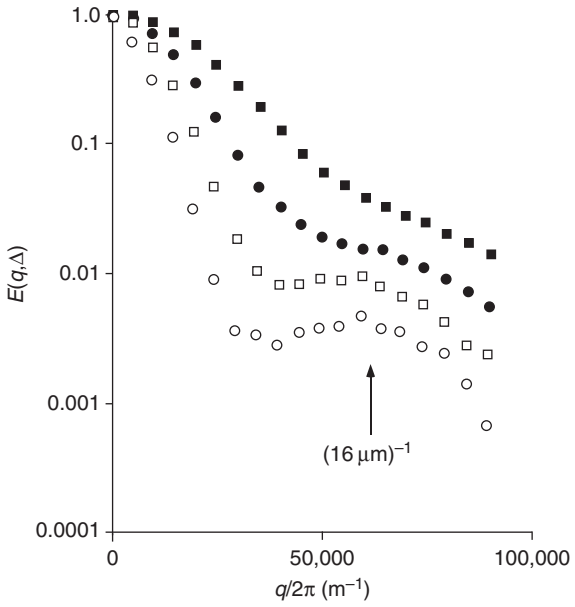

Fig. 7.1 Diffusive diffraction pattern observed for water molecules in a random packing of spherical polymer beads. The data are plotted for increasing values of Δ, 20, 40, 70, and 110 ms. (Adapted from reference [2].)

time, Δ, is increased, a distinct diffraction peak is observed at a reciprocal space value close to the bead diameter value and mean spacing between pores.

In this chapter we outline the physics underlying diffraction effects in PGSE NMR measurements on molecules undergoing restricted motion, providing examples of its application. Of course, a key factor underpinning our description is the narrow gradient pulse condition, since this allows direct access to the propagators for spin displacement. Nonetheless, the condition is not a constraint. We know how to extend our description in the case where gradient pulses are finite. Interpretation of the 'diffractograms' demands a little more care, as coherence effects are dampened and peak positions shifted, but the essential physics remains. Only when the gradient pulse width becomes so long that steady gradient conditions apply do we lose diffraction effects significantly. Such steady gradient experiments in restricted motion were considered in the previous chapter. In this chapter, pulsed gradients take centre stage.

7.1 PGSE NMR 'diffraction' in pores

While the steady gradient spin-echo experiment is capable of revealing the role of restrictions to motion caused by collision of molecules at surfaces bounding the fluid, any detail concerning the shape of those surfaces is buried in numerical prefactors appearing in the exponent of near-Gaussian decays. But in the narrow gradient pulse version of PGSE NMR, where the role of the wavevector $\mathbf{q}$ makes possible the direct sampling of the probability distribution of molecular displacements, a more transparent

structural analysis arises. Furthermore, under conditions in which sufficient echo time is allowed for molecules to be able to diffuse through all the pore space, the echo signal bears a Fourier power spectrum relationship to the sample structure factor [2, 4, 5].

7.1.1 A historical precursor: rectangular boundaries

We start by examining a very simple example in which molecules in the liquid state are confined within a rectangular box with distance a between the boundaries. Suppose that a narrow gradient pulse PGSE experiment is performed with the gradient applied parallel to one side (z) of the box of length a, i.e. $\mathbf{g} = g\hat{\mathbf{k}}$. This problem was solved exactly by Tanner and Stejskal [6] under the assumption of perfectly reflecting boundaries. For the conditional probability they obtained the result

$$P_s(z|z',\Delta) = 1 + 2\sum_{n=1}^{\infty} \exp\left(-\frac{n^2\pi^2 D_0\Delta}{a^2}\right) \cos\left(\frac{n\pi z'}{a}\right) cos\left(\frac{n\pi z}{a}\right) \tag{7.1}$$

with corresponding echo-attenuation function

$$E(g,\Delta) = \frac{2[1-\cos(\gamma g\delta a)]}{(\gamma g\delta a)^2} + 4(\gamma g\delta a)^2 \sum_{n=1}^{\infty} \exp\left(-\frac{n^2\pi^2 D_0\Delta}{a^2}\right) \times \frac{1-(-1)^n\cos(\gamma g\delta a)}{(\gamma g\delta a)^2 - (n\pi)^2} \tag{7.2}$$

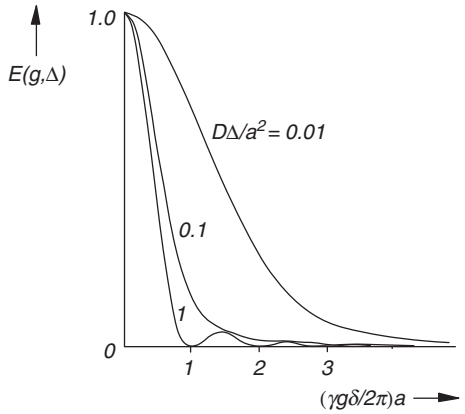

Fig. 7.2 Echo attenuation for diffusion in a box as represented by eqn 7.2. $E(g,\Delta)$ is shown for diffusion times, Δ, both small and comparable with the mean time taken to diffuse across the box, a^2/D_0. For larger values of Δ the behaviour is essentially time-independent and equivalent to that shown for $D_0\Delta/a^2 = 1$.

The short timescale limit ($\Delta \ll a^2/2D_0$) of eqn 7.2 corresponds to the free-diffusion regime of Section 6.5.2, for which $E(g,\Delta) = \exp(-\gamma^2 g^2\delta^2 D_0\Delta)$, while in the long timescale limit ($\Delta \gg a^2/2D_0$)

$$E(g,\Delta) = \frac{2\,(1-\cos(\gamma g \delta a))}{(\gamma g \delta a)^2} \tag{7.3}$$

This result is particularly interesting. First, it is independent of both Δ and D_0. Expanding eqn 7.2 to fourth order in $\gamma g \delta a$ we find

$$\begin{aligned} E(g,\Delta) &\approx 1 - \tfrac{1}{12}(\gamma g \delta a)^2 \\ &\approx \exp(-\gamma^2 g^2 \delta^2 D_{app} \Delta) \end{aligned} \tag{7.4}$$

where $D_{app} = a^2/12\Delta$. Hence the apparent diffusion coefficient decreases as the observation time, Δ, increases. Its magnitude is simply the mean-square distance travelled by the molecules, $a^2/6$, divided by twice the observation time. Note that where the PGSE gradient amplitude is weak ($\gamma g \delta a \ll 1$), we might expect to reproduce the motional narrowing ($l_D/l_s \gg 1$ and $l_g/l_s \gg 1$) regime of Section 6.5.2. But the result is very different from the motional narrowing result, eqn 6.68, found in the case of the steady gradient spin echo. The reason is simply that in the case of infinitesimally narrow gradient pulses, there is no spectral spread to be averaged by the spin diffusion, since the gradient is turned off during the diffusion period Δ. Instead, this idealised narrow pulse experiment measures directly the mean-squared displacement of the molecules.

The second interesting aspect of eqn 7.3 concerns its non-Gaussian character. This idea that the apparent diffusion coefficient, as measured by PGSE, is described by a term of order the mean-squared displacement divided by the timescale, is only true where the gradient applied is weak, meaning that the magnitude of $q = \gamma g \delta$ is much less than the reciprocal of the barrier spacing. The finite gradient form of eqn 7.3 has a very peculiar feature associated with the condition $qa = 2\pi$. Here, the echo signal is completely zero, as if the spins had diffused an infinite distance. The exact behaviour represented by eqn 7.2 is shown in Fig. 7.2. The meaning of the pathological behaviour of $E(q)$ in the case $qa = 2\pi$ will be apparent once we have developed a suitable formalism for the long time limit signal.

7.1.2 Diffusive diffraction in an enclosed pore

Consider the behaviour of molecules enclosed in a pore of volume V described by the magnetisation density function $M(\mathbf{r},t)$, where at time $t = 0$ this magnetisation is uniform and equal to the pore density function, $\rho(\mathbf{r}) = V^{-1}$, inside the pore and zero outside. For the moment, we will presume that the pore surface is perfectly reflecting, or in other words, that there is no special relaxation at the walls and that all loss of magnetisation due to relaxation occurs equally for all molecules. This condition ensures that relaxation effects may be uniformly normalised.

In calculating the NMR signal we need to sum all contributions by integrating over the pore space, as indicated by $\int_V ...d\mathbf{r}$. In fact the V subscript is optional provided that we define the pore density function, $\rho(\mathbf{r})$, to be zero outside the pore. Hence we will often omit this subscript and allow that the integral may be taken over all space.

Memory loss and the pore density assumption

There will be some length scale l_s that characterises the pore size. On a timescale long compared with that taken to diffuse a distance l_s, molecules will have diffused backwards and forwards across the box many times and have lost all 'memory' of their initial positions. In mathematical terms this means that the conditional probability $P(\mathbf{r}|\mathbf{r}', \Delta \to \infty)$ is simply related to the pore geometry.

The loss of memory of starting positions as $D_0\Delta/l_s^2 \to \infty$ is commonly expressed by stating that the probability of finding a molecule at any final coordinates $\mathbf{r}'$ within the pore may be written as $\rho(\mathbf{r}')$. We will soon see that this assumption is not precisely correct, but for the moment, it will serve our purpose.

In Chapter 5 it was shown that $E(\mathbf{q}, \Delta)$ has a Fourier relationship with $\bar{P}(\mathbf{R}, \Delta)$, the probability distribution for displacement $\mathbf{R}$ over time Δ, also known as the 'displacement propagator'. If $P_s(\mathbf{r}|\mathbf{r}', \Delta \to \infty) = \rho(\mathbf{r}')$, then the average propagator has a very special character, namely

$$\bar{P}(\mathbf{R}, \infty) = \int \rho(\mathbf{r} + \mathbf{R})\rho(\mathbf{r})d\mathbf{r}. \tag{7.5}$$

This expression is exactly the auto-correlation function of the molecular density! Figure 7.3 shows $\bar{P}(\mathbf{R}, \infty)$ for the rectangular box example previously considered. Properly normalised, it has the form

$$\begin{aligned} \bar{P}(Z, \infty) = \frac{a + Z}{a^2} \qquad & -a \le Z \le 0 \\ \frac{a - Z}{a^2} \qquad & 0 \le Z \le a \end{aligned} \tag{7.6}$$

We are now in a position to calculate the rectangular box mean-square displacement.

$$\begin{aligned} \langle Z^2 \rangle &= \int_{-\infty}^{\infty} Z^2 \bar{P}(Z, \infty) dZ \\ &= \frac{1}{a^2} \int_{-a}^{0} Z^2(a + Z)dZ + \frac{1}{a^2} \int_{0}^{a} Z^2(a - Z)dZ \\ &= \tfrac{1}{6}a^2 \end{aligned} \tag{7.7}$$

Note the use of the symbol $\langle ....\rangle$ to represent the ensemble average, in this case implicitly over all starting pore positions and all possible particle displacements.

The diffraction relationship

The idea that the long timescale averaged propagator is simply the auto-correlation function of the molecular density, $\rho(\mathbf{r})$, is a very powerful tool. In particular, since the PGSE experiment (in the narrow pulse approximation) gives us a signal $E(\mathbf{q}, \Delta)$ that is simply the Fourier transform of $\bar{P}(\mathbf{R}, \Delta)$, we obtain another important insight. It is well known in the theory of light scattering that the Fourier transform of a time auto-correlation function is simply the frequency power spectrum, a result sometimes known as the Wiener–Khintchine theorem [7]. We shall express this idea in our own

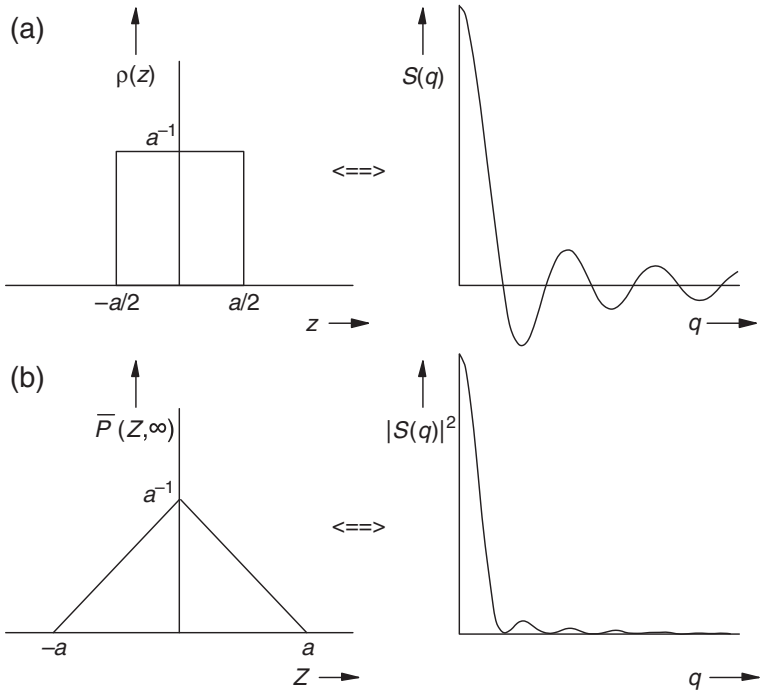

Fig. 7.3 (a) The 1-D density function, $\rho(z)$, for molecules confined to a rectangular box of width a, along with its corresponding Fourier transform, $S(q)$. (b) The infinite time-averaged propagator, $\bar{P}(Z,\infty)$, for the rectangular box and its corresponding transform. Because $\bar{P}(Z,\infty)$ is the auto-correlation function of $\rho(z)$, $\mathcal{F}\{\bar{P}(Z,\infty)\}$ is simply $|S(q)|^2$. In the optical analogy, $|S(q)|^2$ is the diffraction pattern from a single slit.

terms by returning to first principles. In the long-time limit, where $P_s(\mathbf{r}|\mathbf{r}', \Delta \rightarrow \infty)$ reduces to $\rho(\mathbf{r}')$, eqn 5.81 tells us

$$\begin{aligned} E(\mathbf{q},\infty) &= \iint \rho(\mathbf{r})\rho(\mathbf{r}')\exp(i\mathbf{q}\cdot(\mathbf{r}'-\mathbf{r}))d\mathbf{r}d\mathbf{r}' \\ &= \int \rho(\mathbf{r})\exp(-i\mathbf{q}\cdot\mathbf{r})d\mathbf{r}\int \rho(\mathbf{r}')\exp(i\mathbf{q}\cdot\mathbf{r}')d\mathbf{r}' \\ &= S^*(\mathbf{q})S(\mathbf{q}) \\ &= |S(\mathbf{q})|^2 \end{aligned} \tag{7.8}$$

$S(\mathbf{q})$ is known as the 'structure factor' and is sometimes denoted $\tilde{\rho}(\mathbf{q})$.

Eqn 7.8 states that in the very long time limit, when the molecules move over the entire sample, the PGSE signal is precisely the power spectrum of the structure factor, an optical analogy pointed out by Cory and Garroway [4]. This is a remarkable result because it means that the PGSE experiment in the long-time limit is an imaging experiment in its own right, returning not the structure factor as in k-space imaging, but the modulus squared of the structure factor. The loss of phase information by

this squaring process is a severe disadvantage but it is exactly the price paid in X-ray diffraction experiments. There, the intensity structure factor is interpreted by comparing it with that calculated from a starting model in real space. But in one crucial aspect, PGSE or q-space static imaging has a major advantage over the k-space method in NMR microscopy. Because the signal is sampled in the absence of a gradient, there is no fundamental resolution limit! The only limit is imposed by the magnitude of the pulsed gradient that can be applied, subject to the condition that the two gradient pulses must be well-matched in area.

The rectangular box and single-slit diffraction

Equation 7.8 can be used to give a nice description of the long timescale behaviour in the rectangular box. The structure factor, $S(q)$, for the rectangular box is simply the Fourier transform of a hat function, as shown in Fig. 7.3. Thus

$$\begin{aligned} E(\mathbf{q},\infty) &= |sinc(\tfrac{1}{2}qa)|^2 \\ &= \frac{4\sin^2(\tfrac{1}{2}qa)}{(qa)^2} \\ &= \frac{2(1-cos(qa))}{(qa)^2} \end{aligned} \tag{7.9}$$

This is exactly the result of eqn 7.3, an equivalence which can be seen by comparison of Fig. 7.3(b) and the long timescale limit of Fig. 7.2. Its optical analogue is the diffraction pattern of a single slit where the origin of the node when $qa = 2\pi$ is phase cancellation arising from different 'slit elements' across the uniform density, $\rho(z)$, of width a. For single-slit diffraction, each element at z with resulting phase shift $\exp(iqz)$ has an equivalent corresponding element at $(a/2 + z)$, with phase shift $\exp(iq(a/2 + z))$ or $-\exp(iqz)$. For diffusive diffraction, where the density $P(Z)$ is not uniform but given by the autocorrelation function of $\rho(z)$, the same values of q cause cancellation in the sum of elements weighted by their respective phase shifts.

Diffraction from a sphere

It is useful to apply the structure factor idea to other structures in which bounded diffusion occurs. The long timescale behaviour for particles diffusing in a sphere of radius a can be obtained by calculating the 1-D Fourier transform of the normalised density. This latter function is simply $(3/4a^3)(z^2 - a^2)$ for $-a \leq z \leq a$ and zero elsewhere. Thus

$$\begin{aligned} S(q) &= \int_{-a}^{a} \frac{3}{4a^3}(z^2 - a^2)\exp(iqz)dz \\ &= \frac{3[qa\cos(qa) - \sin(qa)]}{(qa)^2} \end{aligned} \tag{7.10}$$

The PGSE signal, $E(q,\infty)$, is $|S(q)|^2$ and has a node when $qa \approx 3/4$. The behaviour when $qa \ll 2\pi$ is

$$\begin{aligned} E(q) &\approx 1 - \frac{1}{5}(qa)^2 \\ &\approx \exp(-\tfrac{1}{5}\gamma^2 g^2 \delta^2 a^2) \end{aligned} \tag{7.11}$$

In fact eqn 7.11 gives quite a good description of $E(q,\infty)$ over a decade of attenuation ($qa \leq \pi$). Comparison with eqn 5.90 shows that the weak gradient apparent diffusion coefficient is $a^2/5\Delta$. As in the case of the rectangular box, this is the mean-square distance diffused by the molecules, $(2/5)a^2$, divided by 2Δ.

7.1.3 The pore density assumption revisited

Suppose we investigate the long-time limit via the molecular probability density $p(\mathbf{r},t)$, where we allow that $p(\mathbf{r},0) = \rho(\mathbf{r})$, and, because of the long term equilibration within the pore, $p(\mathbf{r},\infty) = \rho(\mathbf{r})$. Again, we will, for the moment, neglect wall relaxation effects and assume that the boundaries are perfectly reflecting. Using the eigenmode expansion

$$p(\mathbf{r},t) = \sum_n A_n u_n(\mathbf{r}) \exp(-Dk_n^2 t) \tag{7.12}$$

it follows that

$$\rho(\mathbf{r}) = \sum_n A_n u_n(\mathbf{r}) \tag{7.13}$$

Because of the orthogonality of the $\{u_m\}$, $A_m = \int_V \rho(\mathbf{r}) u_m^*(\mathbf{r}) d\mathbf{r}$. It is easy to show that for perfectly reflecting walls, $k_m \neq 0$ except for $m = 0$, so that we have

$$p(\mathbf{r},\infty) = \left(\int_V \rho(\mathbf{r}') u_0^*(\mathbf{r}') d\mathbf{r}' \right) u_0(\mathbf{r}) \tag{7.14}$$

And since $p(\mathbf{r},\infty) = \rho(\mathbf{r})$, we are able to identify the lowest eigenmode as proportional to the pore density function via

$$\begin{aligned} u_0(\mathbf{r}) &= \frac{\rho(\mathbf{r})}{\int_V \rho(\mathbf{r}') u_0^*(\mathbf{r}') d\mathbf{r}'} \\ \therefore \int_V \rho(\mathbf{r}) u_0(\mathbf{r}) d\mathbf{r} \times \int_V \rho(\mathbf{r}') u_0^*(\mathbf{r}') d\mathbf{r}' &= \int_V \rho(\mathbf{r})^2 d\mathbf{r} \end{aligned} \tag{7.15}$$

Next, we turn our attention to the conditional probability. Given

$$P(\mathbf{r}|\mathbf{r}',\Delta) = \sum_n u_n^*(\mathbf{r}) u_n(\mathbf{r}') \exp(-Dk_n^2 t) \tag{7.16}$$

it is clear that pore equilibration leads to

$$\begin{aligned} P(\mathbf{r}|\mathbf{r}',\Delta \to \infty) &= u_0^*(\mathbf{r}) u_0(\mathbf{r}') \\ &= \frac{\rho(\mathbf{r})\rho(\mathbf{r}')}{\int_V \rho(\mathbf{r})^2 d\mathbf{r}} \end{aligned} \tag{7.17}$$

In consequence, the simple diffusive diffraction relationship represented by eqn 7.8 must be rewritten[2]

[2]The author is grateful to Charles Epstein, of the University of Pennsylvania, for pointing this out.

$$E(\mathbf{q},\infty) \propto \iint \rho(\mathbf{r})^2 \rho(\mathbf{r}') \exp(i\mathbf{q}\cdot(\mathbf{r}'-\mathbf{r}))d\mathbf{r}d\mathbf{r}' \tag{7.18}$$

and so the echo attenuation does not have the simple $|S(\mathbf{q})|^2$ form as commonly assumed. Does it really matter? If the pore density is uniform, in other words if $\rho(\mathbf{r}) = 1/V$, then $\rho(\mathbf{r})^2 \propto \rho(\mathbf{r})$ and of course eqn 7.18 is indistinguishable from eqn 7.8. In every experimental case examined so far, this simple identity holds. But could one envisage a problem where $\rho(\mathbf{r})$ is non-uniform? Of course, it is possible to begin a diffusive diffraction experiment with a non-uniform magnetisation, for example by allowing wall relaxation in advance of the application of the first magnetic field gradient pulse. This initial distribution would have to be accounted for in any calculation. But where the intrinsic spin density varies, for example due to an inhomogeneous distribution of permeable barriers, as one might find when imaging biological tissue, the problem will be further complicated by heterogeneous diffusion rates.

Certainly for liquids imbibed in any porous matrix where the fluid phase is homogeneous, the simple diffusive diffraction relation, eqn 7.8, applies, provided asymptotic pore equilibration conditions are reached. In the next section we see how to treat the PGSE NMR experiment under restricted diffusion conditions at all timescales and under conditions of wall relaxation.

7.1.4 Diffusive diffraction in a matrix of enclosing pores

Suppose that instead of a single pore, our sample consists of a matrix of N pores, labelled by i, as shown in figure 7.4, where each pore centre is given by a vector $\mathbf{r}_{0i}$ while each pore density function is $\rho_{0i}(\mathbf{r}-\mathbf{r}_{0i})$. The zero subscript distinguishes the local pore density function from the overall sample density. For convenience we define a local pore coordinate $\mathbf{r}_p = \mathbf{r} - \mathbf{r}_{0i}$.

The normalised spin echo signal in the narrow gradient pulse approximation can be written

$$\begin{aligned}
E(\mathbf{q},\infty) &= \frac{1}{N}\sum_{i=1}^{N} \int \rho_{0i}(\mathbf{r}-\mathbf{r}_{0i}) \exp(-i\mathbf{q}\cdot\mathbf{r})d\mathbf{r} \int \rho_{0i}(\mathbf{r}'-\mathbf{r}_{0i}) \exp(i\mathbf{q}\cdot\mathbf{r}')\ d\mathbf{r}' \\
&= \frac{1}{N}\sum_{i=1}^{N} \int \rho_{0i}(\mathbf{r}_p) \exp(-i\mathbf{q}\cdot(\mathbf{r}_{0i}+\mathbf{r}_p))d\mathbf{r}_p \int \rho_{0i}(\mathbf{r}'_p) \exp(i\mathbf{q}\cdot(\mathbf{r}_{0i}+\mathbf{r}'_p))\ d\mathbf{r}'_p \\
&= \frac{1}{N}\sum_{i=1}^{N} \int \rho_{0i}(\mathbf{r}_p) \exp(-i\mathbf{q}\cdot\mathbf{r}_p)d\mathbf{r}_p \int \rho_{0i}(\mathbf{r}'_p) \exp(i\mathbf{q}\cdot\mathbf{r}'_p)d\mathbf{r}'_p \\
&= \frac{1}{N}\sum_{i=1}^{N} S^*_{0i}(\mathbf{q}) S_{0i}(\mathbf{q}) \\
&= \overline{|S_0(\mathbf{q})|^2}
\end{aligned} \tag{7.19}$$

Hence the diffusive diffraction experiment returns the averaged squared structure factor for the pores. Fourier transformation of this echo signal yields to averaged pore correlation function, since

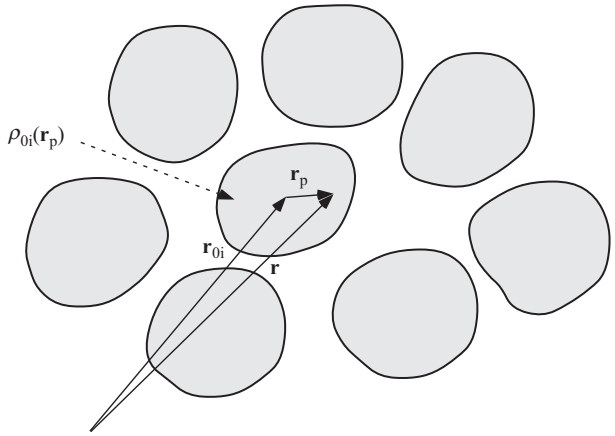

Fig. 7.4 A porous medium consisting of a matrix of similar pores, characterised by centre coordinates $\mathbf{r}_{0i}$, local pore coordinates $\mathbf{r}_p$ and pore densities $\rho_{0i}(\mathbf{r}_p)$.

$$\mathcal{F}\{\overline{|S_0(\mathbf{q})|^2}\} = \overline{\int \rho_0(\mathbf{r}_p)\rho_0(\mathbf{r}_p + \mathbf{R})d\mathbf{r}_p} \tag{7.20}$$

At first sight the result seems unremarkable in comparison with eqns 7.5 and 7.8. But note that the cancellation of the pore centre coordinates leads to a result in which the structure revealed is that of an 'average pore' rather than the whole sample itself. The Fourier transform of the signal gives a kind of averaged pore image, albeit an image of the pore correlation function rather than the pore itself. But the crucial point is that the field of view (FOV) for that image will have dimensions comparable with the pore size rather than the sample size. In standard MRI experiments, the available signal must be distributed between the various voxels of the image, thus limiting the number of voxels available, since the voxel signal-to-noise ratio decreases as the number of voxels increase. Suppose the sample allows as many N_V voxels, with acceptable signal-to-noise ratio. Then the image resolution will be $FOV/N_V^{1/n}$ for an n-dimensional image. In the diffusive diffraction experiment the potential resolution is therefore very much better, allowing for voxel sizes on the order of microns or even smaller. That is the real power of the diffusive diffraction method in the elucidation of sample structure.

This result begs the question as to whether there exists the equivalent of an imaging experiment in a matrix of enclosed pores, in which the field of view remains on the order of the pore size, rather than the sample size, while the image returned is that of the averaged pore rather than the averaged pore correlation function. Indeed there is such an experiment.

7.1.5 'Long-narrow' PGSE NMR: direct imaging of the structure factor by diffusive diffraction

Laun *et al.* [8] have proposed an ingenious adaptation of the PGSE NMR experiment that provides a solution to the problem of the loss of phase information in the standard

narrow gradient pulse diffusive diffraction experiment for which $\overline{|S_0(\mathbf{q})|^2}$ is returned. Their variant, shown in Fig 7.5, exchanges the narrow first effective gradient pulse with an equal area long pulse, and of duration T such that $T \gg l_s^2/D$. The pulse sequence might be labelled 'long-narrow' PGSE NMR.

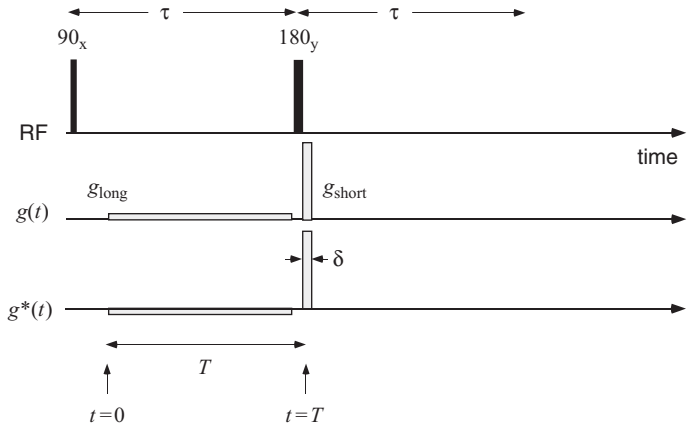

Fig. 7.5 Modified two-pulse PGSE NMR experiment ('long-narrow' PGSE NMR) due to Laun *et al* [8] in which the first narrow gradient pulse is replaced by a weak long pulse of duration T and of equal area. Hence $\mathbf{q} = \gamma T \mathbf{g}_{long} = \gamma \delta \mathbf{g}_{short}$.

Eqn 7.19 tells us that the two-pulse narrow gradient experiment returns the average value of individual pore terms $S_0(\mathbf{q})^* S_0(\mathbf{q})$. The same sort of multipore sample average will be returned by the experiment shown in Fig 7.5. To understand the meaning of the new experiment, we therefore only need to focus on a single pore.

$$E(\mathbf{q},T) = \int \rho_0\big(\mathbf{r}(0)-\mathbf{r}_0\big)\exp\big(-i\mathbf{q}\cdot\frac{1}{T}\int_0^T \mathbf{r}(t)dt\big)d\mathbf{r}(0) \times \int \rho_0\big(\mathbf{r}(T)-\mathbf{r}_0\big)\exp\big(i\mathbf{q}\cdot\mathbf{r}(T)\big)d\mathbf{r}(T) \tag{7.21}$$

Note that the final coordinate sampled by the second, narrow, gradient pulse is $\mathbf{r}' = \mathbf{r}(T)$, the position of a molecule at the end of the first, long pulse. To simplify our notation, let us replace $\int \rho_0(\mathbf{r}-\mathbf{r}_0)....d\mathbf{r}$ by $\big\langle....\big\rangle$. Then

$$\begin{aligned} E(\mathbf{q},T) &= \Big\langle \exp\big(-i\mathbf{q}\cdot\frac{1}{T}\int_0^T \mathbf{r}(t)dt\big)\exp\big(i\mathbf{q}\cdot\mathbf{r}(T)\big)\Big\rangle \\ &= \Big\langle \exp\big(-i\mathbf{q}\cdot\frac{1}{T}\int_0^T [\mathbf{r}_0+\mathbf{r}_p(t)]dt\big)\exp\big(i\mathbf{q}\cdot[\mathbf{r}_0+\mathbf{r}_p(T)]\big)\Big\rangle \\ &= \Big\langle \exp\big(-i\mathbf{q}\cdot\frac{1}{T}\int_0^T \mathbf{r}_p(t)dt\big)\exp\big(i\mathbf{q}\cdot\mathbf{r}_p(T)\big)\Big\rangle \end{aligned} \tag{7.22}$$

Laun *et al.* note that for T long compared with the time to diffuse back and forth across a pore, the time integral of $\mathbf{r}_p(t)$ is approximately T multiplied by the time averaged (pore centre) coordinate, and in the present notation, where we choose the coordinate origin at the pore centre, that value is zero. Assuming that the ensemble average may be shifted to the exponent, Laun *et al.* find $E(\mathbf{q},\infty) = \langle \exp\big(i\mathbf{q}\cdot\mathbf{r}_p(T)\big)\rangle = S_0(\mathbf{q})$, so that this new experiment apparently returns the pore structure factor directly. The great advantage of this experiment is that an image of the averaged pore density function, $\rho(\mathbf{r}_p)$, can be directly computed via a Fourier transformation.

Careful analysis suggests that this structure factor could be multiplied by a further attenuation factor (and hence the image blurred) due to motion occurring during the first long gradient pulse. We need to perform the correct ensemble average of the phase factors to find any additional attenuation factor multiplying $S_0(\mathbf{q})$.

Before obtaining this factor, it is interesting to evaluate the echo attenuation obtained using pulse sequence of Fig 7.5 in the case of free diffusion. By making the substitution $\mathbf{r}_p(t) = \mathbf{r}_p(0) + \mathbf{R}(t)$ and noting $\mathbf{r}_p(T) = \mathbf{r}_p(0) + \mathbf{R}(T)$, eqn 7.22 becomes

$$\begin{aligned} E(\mathbf{q},T) &= \langle \exp\big(-i\mathbf{q}\cdot\frac{1}{T}\int_0^T \mathbf{R}(t)dt\big)\exp\big(i\mathbf{q}\cdot\mathbf{R}(T)\big)\rangle \\ &= \langle \exp\big(-iq\frac{1}{T}\int_0^T Z(t)dt\big)\exp\big(iqZ(T)\big)\rangle \end{aligned} \tag{7.23}$$

To evaluate eqn 7.23 we need to know whether $\int_0^T Z(t)dt$ and $Z(T)$ are correlated or uncorrelated. For free diffusion $\int_0^T Z(t)dt$ and $Z(T)$ are indeed correlated[3] and $\langle \int_0^T Z(t)dtZ(T)\rangle = DT^2$. The easiest way to handle the ensemble average problem in the case of the weak steady gradient is to use the Gaussian phase approximation, in other words to write the solution as $\exp(-\frac{1}{2}q^2\sigma_\chi^2)$ where σ_χ^2 is the mean-squared average of the term in square brackets, i.e.

$$\begin{aligned} \sigma_\chi^2 &= \langle\big(\frac{1}{T}\int_0^T Z(t)dt - Z(T)\big)^2\rangle \\ &= \langle\big(\frac{1}{T}\int_0^T Z(t)dt\big)^2\rangle - \langle 2\big(Z(T)\frac{1}{T}\int_0^T Z(t)dt\big)^2 + \langle Z(T)^2\rangle \end{aligned} \tag{7.24}$$

We met $\langle\big(\int_0^T Z(t)dt\big)^2\rangle$ before in the Carr-Purcell evaluation of steady gradient effects in eqn 5.43. It has the value $\frac{2}{3}DT^3$. Given $\langle Z(T)^2\rangle = 2DT$, $\exp\big(-\frac{1}{2}q^2\sigma_\chi^2\big) = \exp\big(-\frac{1}{3}q^2DT\big)$ for free diffusion.

The interpretation of eqn 7.24 when the diffusion is restricted in a pore of size l_s is quite subtle. Suppose a particle starts at coordinate $z_p(0)$. Then for large T, it will have diffused back and forth across the pore many times such that it may, with equal probability, finish up anywhere in the pore so that $\langle z_p(T)\rangle = 0$ and $\langle \int_0^T Z dt\rangle = -z_p(0)$. Thus the cancellation of starting pore positions which led to eqn 7.24 is no

[3]The problem may be evaluated by noting $(\partial/\partial T)(\int_0^T Z(t)dt)^2 = 2Z(T)\int_0^T Z(t)dt$ and $(\partial/\partial T)Z(T)\int_0^T Z(t)dt = Z^2(T) + \ddot{Z}\int_0^T Z(t)dt$, the ensemble average of the second term being zero as discussed in section 1.3.7.

longer helpful and we need to return to our absolute pore position notation of eqn 7.22. Noting that the final coordinate $z_p(T)$ is completely uncorrelated with prior particle positions,

$$E(q,T) = \left\langle \exp\left(-iq\frac{1}{T}\int_0^T z_p(t)dt\right)\exp\left(iqz_p(T)\right)\right\rangle$$
$$= \left\langle \exp\left(-iq\frac{1}{T}\int_0^T z_p(t)dt\right)\right\rangle S_0(q) \qquad (7.25)$$

And so the pore structure factor is indeed measured, although multiplied by the additional attenuation factor $\left\langle \exp\left(-iq\frac{1}{T}\int_0^T z_p(t)dt\right)\right\rangle$. Again, we use the Gaussian phase approximation, and thus calculate $\sigma_\chi^2 = \left\langle\left(\frac{1}{T}\int_0^T z_p(t)dt\right)^2\right\rangle$. This may be evaluated from a knowledge of the conditional probability $P(z_p(0)|z_p(T),T)$. Let us do this calculation for a simple rectangular pore of width $l_s = 2a$ for which z_p ranges from $-a$ to a. The conditional probability is given in eqn 7.27 and after some algebra, we find $\sigma_\chi^2 = 4(a^2/(\frac{\pi}{2})^6)(a^2/DT)$ which vanishes as $T \gg a^2/D$.

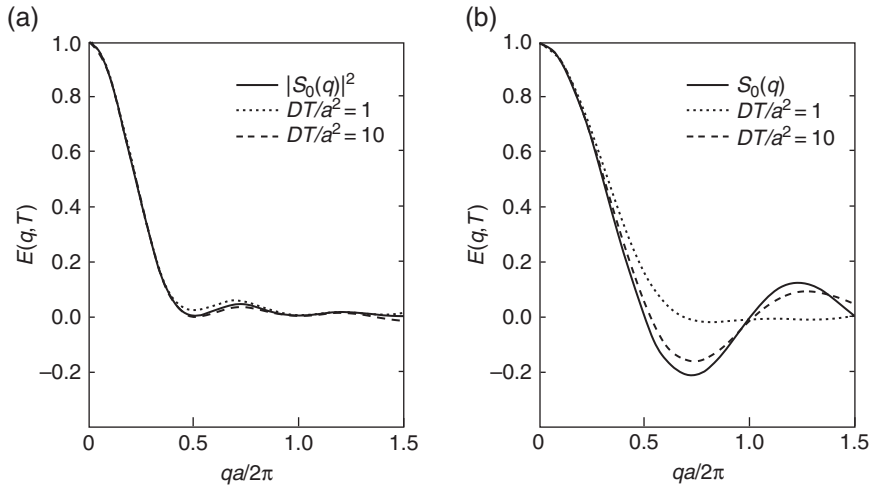

Fig. 7.6 Comparison of simulated echo attenuations, $E(q,T)$, for spins diffusing between rectangular barriers, in the case of the (a) narrow pulse and (b) 'long-narrow' versions of PGSE NMR. 1000 particles are used and the two diffusion times shown correspond to DT/a^2 values of 1 and 10.

The blurring of the image therefore disappears provided we make the diffusion time sufficiently greater than the time to diffuse across a pore. This conclusion is verified in the simulation shown in Fig 7.6 where the results of narrow PGSE pair and 'long-narrow' PGSE NMR for two different diffusion times are compared.

Despite the elegance of long-narrow PGSE NMR, it implies two experimental challenges. First, in stepping the value of q, one must do so with two very differently shaped pulses while scrupulously maintaining the equal area condition. Second, the approach to the asymptotic $S_0(q)$ form as T increases appears slower than that of the

standard narrow pulse PGSE method approaching $|S_0(q)|^2$. These challenges, if met, may be rewarded by the greater information content of $S_0(q)$.

7.2 Finite time diffraction in planar, cylindrical and spherical pores

7.2.1 Finite Δ: the exact treatment

If our interpretation of diffusive diffraction effects were to be restricted to the condition $\Delta \gg l_s^2/D$ and to structures with perfectly reflecting walls, then we would indeed be severely constrained. Wall relaxation effects are a fact of life. Furthermore, the upper limit imposed by spin relaxation to observation time Δ, may, in large pores, make the '$\Delta \to \infty$' condition impossible, while in interconnected porous media, multiple length scales will certainly make this condition difficult to achieve. Yet diffraction effects are still manifest when Δ is finite, as is apparent in Fig. 7.1.

What is needed is a theory more sophisticated than that provided by eqn 7.8 alone, notwithstanding the useful physical insight that this simple limiting case provides. Here we will outline theories which account for finite diffusion times and wall relaxation.

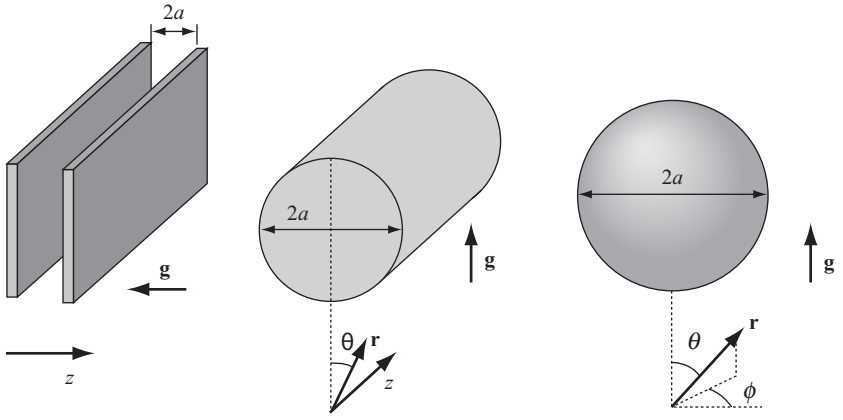

Fig. 7.7 Plane parallel pore, cylindrical pore, and spherical pore, showing relevant dimensions and coordinate frames.

In order to understand the key physics behind the diffusive diffraction phenomenon, it is helpful to show what happens for molecules diffusing in three simple standard geometries, between plane parallel boundaries, and in cylindrical and spherical pores. These are exactly the geometries considered by Brownstein and Tarr in the context of relaxation phenomena, and as part of the analysis presented here, wall relaxation effects will be allowed for. Note that in each case considered, a single pore length scale is relevant,[4] and while these ideal pore shapes may be special cases, they will provide a unique opportunity to calculate closed-form analytic expressions, since each of these boundary conditions leads to well-known eigenmodes of the diffusion equation.

[4]For the plane boundaries and for the cylindrical pore, we shall only be interested in diffusion normal to the pore surface.

A narrow pulse approximation expression for $E(q, \Delta)$ in the case of rectangular pores with relaxing walls was was first published in 1992 by Mitra and Sen [9], although a more complicated, independently derived expression was later published by Snaar and Van As [10] in 1993. The cylindrical pore case was first obtained in 1995 [11], while a formula for $E(q, \Delta)$ in the case of spherical pores was published in reference [9] and corrected in reference [11].

The derivations of the echo-attenuation expressions in each case start with finding the spatial part of the conditional probability, $P(\mathbf{r}|\mathbf{r}', t)$, $u_n(\mathbf{r})$. That is achieved by finding the eigen-solutions to the Helmholtz equation, $\nabla^2 u_n = \lambda_n u_n$, taking advantage of any symmetry, and allowing for the appropriate boundary conditions. To satisfy Fick's second law, the temporal part of each term in the eigenmode expansion is simply $\exp(D_0 \lambda_n t)$, and, as explained in Chapter 1, a finite solution as $t \to \infty$ requires a negative exponent, namely $\lambda_n = -k_n^2$.

7.2.2 Parallel plane pore

This is a 1-D problem in which the gradient is applied along the z-direction normal to a pair of bounding planes, and these relaxing planes are separated by a distance $2a$ and placed at $z = \pm a$.[5] The Helmholtz equation eigenmodes for planar geometry are

$$u_n(z) = \left\{ \begin{array}{c} \cos(\xi_n z) \\ \sin(\zeta_n z) \end{array} \right\} \tag{7.26}$$

The eigenfunction expansion for the propagator is given by

$$\begin{aligned} P(z|z', \Delta) = a^{-1} \sum_{n=0}^{\infty} & \exp(-\frac{\xi_n^2 D\Delta}{a^2})(1 + \sin(2\xi_n)/2\xi_n)^{-1} \\ & \times \cos(\xi_n z/a) \cos(\xi_n z'/a) \\ & + a^{-1} \sum_{m=0}^{\infty} \exp(-\frac{\zeta_m^2 D\Delta}{a^2})(1 - \sin(2\zeta_m)/2\zeta_m)^{-1} \\ & \times \sin(\zeta_m z/a) \sin(\zeta_m z'/a) \end{aligned} \tag{7.27}$$

where the eigenvalues ξ_n and ζ_m are determined by the equations

$$\xi_n \tan(\xi_n) = \frac{\bar{\rho} a}{D} \tag{7.28}$$

and

$$\zeta_m \cot(\zeta_n) = -\frac{\bar{\rho} a}{D} \tag{7.29}$$

The above expression for the conditional probability leads directly to the echo attenuation

[5]Note our preference in denoting the spacing between the plates as $2a$ rather than a, which arises from a desire to more directly compare with the case of the cylinder and sphere, where a is taken to be the radius.

$$E(q,\Delta) = \sum_{n=0}^{\infty} \exp(-\frac{\xi_n^2 D\Delta}{a^2}) 2(1+\sin(2\xi_n)/2\xi_n)^{-1} \times \frac{[(qa)\sin(qa)\cos\xi_n - \xi_n\cos(qa)\sin\xi_n]^2}{[(qa)^2-\xi_n^2]^2} + \sum_{m=0}^{\infty} \exp(-\frac{\zeta_m^2 D\Delta}{a^2}) 2(1-\sin(2\zeta_m)/2\zeta_m)^{-1} \times \frac{[(qa)\cos(qa)\sin\zeta_m - \zeta_m\sin(qa)\cos\zeta_m]^2}{[(qa)^2-\zeta_m^2]^2} \tag{7.30}$$

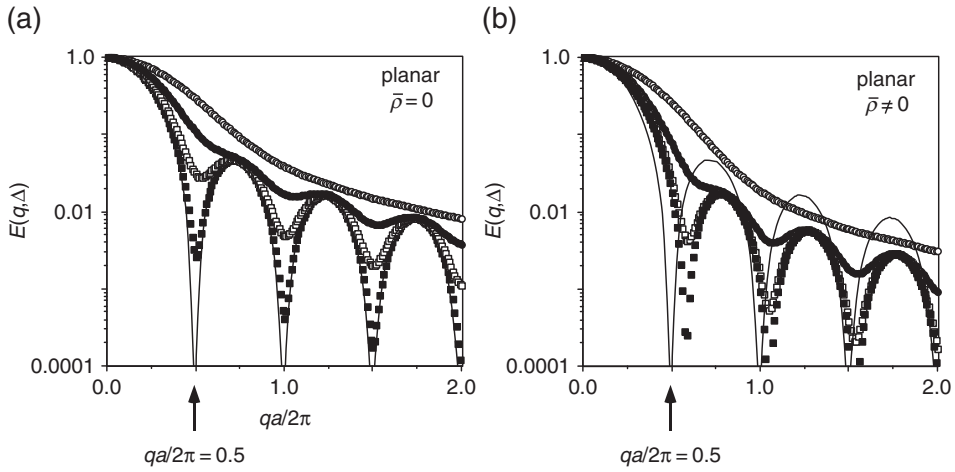

Fig. 7.8 (a) Echo attenuation, $E(q,\Delta)$, for spins trapped between parallel plane barriers separated by $2a$, in which the gradient is applied normal to the planes, and for perfectly reflecting walls ($\bar{\rho}a/D = 0$). Four successive time intervals are displayed. In multiples of a^2/D, Δ is, respectively, 0.2 (open circles), 0.5 (solid circles), 1.0 (open squares), and 2.0 (solid squares). Also shown is the theoretical curve for the infinite time diffraction pattern. Note that the first diffraction minimum occurs near $qa \approx \pi$. (b) as for (a) but for partially absorbing walls ($\bar{\rho}a/D = 2$).

The validity of eqn 7.30 may be checked in two ways. First, it reproduces the standard planar pore relaxation expression of Brownstein and Tarr when $q = 0$. Second, setting $\bar{\rho} = 0$ and noting our different definition of the dimension a, eqn 7.30 reproduces the well-known narrow gradient pulse echo attenuation result of Tanner and Stejskal [6] for rectangular pores with perfectly reflecting walls.

Figure 7.8 shows echo attenuations calculated using eqn 7.30 for a range of echo times both with and without wall relaxation. At times short compared with that required to diffuse between the walls, the echo attenuation is approximately Gaussian. At longer times, as wall collisions start to dominate, distinct diffraction effects are

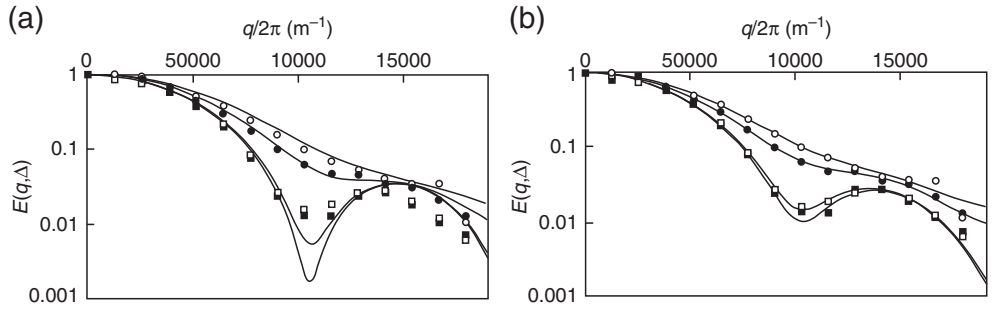

Fig. 7.9 (a) Echo attenuation, $E(q, \Delta)$, obtained in a narrow gradient pulse PGSE NMR experiment using a stack of pentane-filled rectangular capillaries with $2a = 100\mu m$, at different fixed times, Δ, of 200 ms (open circles), 300 ms (closed circles), 700 ms (open squares), and 900 ms (closed squares), and corresponding to the range $0.4a^2/D$ to $1.8a^2/D$. Superposed are theoretical curves obtained from eqn 7.30, in which the known system parameters are used, including $\bar{\rho} = 0.00005$ corresponding to the known T_1. (b) As for (a) but where a distribution of a values is allowed and the system parameters are fitted. (Adapted from reference [12].)

observed. Note the characteristic echo minimum at $qa = \pi$, as well as the fact that the first diffraction maximum occurs at quite a significant degree of echo attenuation where $E(q, \Delta) < 0.1$. The effect of relaxation, apparent in Fig. 7.8(b), is to shift the diffraction minimum to higher q values, suggesting a reduction in the apparent pore size.

Figure 7.9 shows the results of narrow gradient pulse PGSE NMR experiments [12] carried out on pentane molecules diffusing between the walls of a stack of rectangular microcapillaries of spacing $2a = 100\,\mu m$, both with theoretical curves based on the known system parameters and where the parameters are adjusted to allow the best fit for each Δ-value dataset. In the latter case, a is within a few per cent of the manufacturer's specification, while the alignment/spacing standard deviation value is less than 5%. D_0 values, which arise predominantly from the fit to the low q part of the data, are all close to the known self-diffusion coefficient of pentane at 28°C, $5 \times 10^{-9} m^2 s^{-1}$. Note that in the case of the plane parallel pore, the size of the coherence effects is remarkable, with more than a doubling of the echo amplitude with increasing gradient from the minimum near $qa/2\pi = 0.5$ to the maximum near $qa/2\pi = 0.75$.

7.2.3 Cylindrical pore

This is a 2-D problem handled in cylindrical polar coordinates in which the longitudinal z-axis is a symmetry axis for the system. The relevant coordinates are (r, θ) and the gradient is applied along the polar axis direction (i.e. across a diameter). The relaxing boundary is at a radial distance $r = a$ from the cylinder's central axis.

The Helmholtz eigenmodes are

$$u_n(r,\theta) = \left\{ \begin{array}{c} J_n(\beta_{nk}r) \\ N_n(\beta_{nk}r) \end{array} \right\} \left\{ \begin{array}{c} \cos(n\theta) \\ \sin(n\theta) \end{array} \right\} \tag{7.31}$$

where J_n and N_n are Bessel functions of the first and second kind. Since $N_n(\beta_{nk}r)$ diverges as $r \to 0$, only the $J_n(\beta_{nk}r)$ solution is permitted for a cylindrical pore. The eigenfunction expansion for the propagator is given by

$$\begin{aligned} P(\mathbf{r}|\mathbf{r}',\Delta) = \sum_{n,k}^{\infty} \exp(-\frac{\beta_{nk}^2 D\Delta}{a^2}) J_n(\beta_{nk}r/a) J_n(\beta_{nk}r'/a) \\ \times A_{nk}^2 \cos(n\theta)\cos(n\theta') \end{aligned} \tag{7.32}$$

where for $n \neq 0$

$$A_{nk}^2 = \frac{(2/\pi a^2)(\beta_{nk}^2/J_n^2(\beta_{nk}))}{(\bar{\rho}a/D)^2 + \beta_{nk}^2 - n^2} \tag{7.33}$$

and

$$A_{0k}^2 = \frac{(1/\pi a^2)(\beta_{0k}^2/J_0^2(\beta_{0k}))}{(\bar{\rho}a/D)^2 + \beta_{0k}^2} \tag{7.34}$$

The J_n are standard (cylindrical) Bessel functions, while the eigenvalues β_{nk} are determined by the equations

$$\beta_{nk}\frac{J_n'(\beta_{nk})}{J_n(\beta_{nk})} = -\frac{\bar{\rho}a}{D} \tag{7.35}$$

From eqn 7.32, the echo-attenuation expression follows

$$\begin{aligned} E(q,\Delta) = \sum_{k}^{\infty} 4\exp(-\frac{\beta_{0k}^2 D\Delta}{a^2}) \frac{\beta_{0k}^2}{(\bar{\rho}a/D)^2 + \beta_{0k}^2} \\ \times \frac{\left[(qa)J_0'(qa) + (\bar{\rho}a/D)J_0(qa)\right]^2}{\left[(qa)^2 - \beta_{0k}^2\right]^2} \\ + \sum_{nk}^{\infty} 8\exp(-\frac{\beta_{nk}^2 D\Delta}{a^2}) \frac{\beta_{nk}^2}{(\bar{\rho}a/D)^2 + \beta_{nk}^2 - n^2} \\ \times \frac{\left[(qa)J_n'(qa) + (\bar{\rho}a/D)J_n(qa)\right]^2}{\left[(qa)^2 - \beta_{nk}^2\right]^2} \end{aligned} \tag{7.36}$$

As required by setting $q = 0$, eqn 7.36 reproduces the Brownstein–Tarr result for relaxation within cylindrical pores. The spin-echo-attenuation result for perfectly reflecting cylindrical pores was independently derived by Linse and Söderman [14] and eqn 7.36 reduces to their result when $\bar{\rho} = 0$.

Figure 7.10 shows echo attenuations calculated using eqn 7.36 for a range of echo times both with and without wall relaxation. The phenomena are similar to those

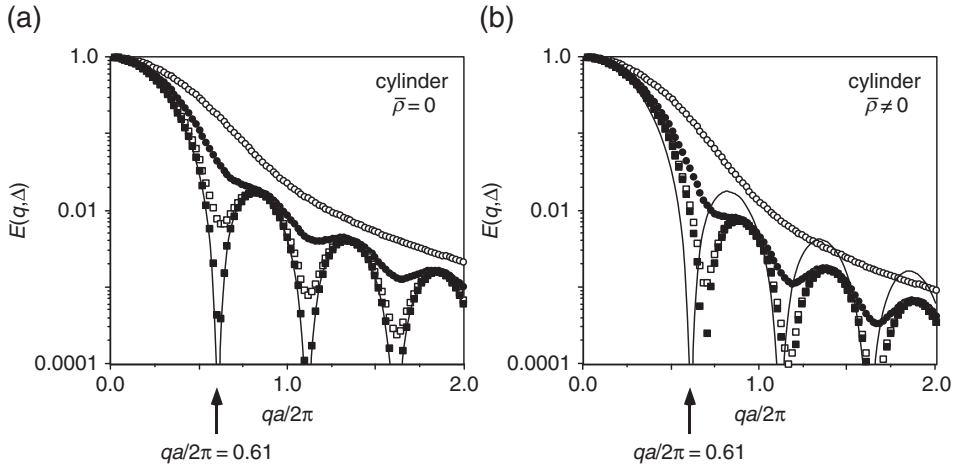

Fig. 7.10 (a) Echo attenuation, $E(q, \Delta)$, for spins trapped in a cylindrical pore of radius a in which the gradient is applied across a diameter and for perfectly reflecting walls ($\bar{\rho}a/D = 0$). Four successive time intervals are displayed. In multiples of a^2/D, Δ is, respectively, 0.2 (open circles), 0.5 (solid circles), 1.0 (open squares), and 2.0 (solid squares). Also shown is the theoretical curve for the infinite time diffraction pattern. Note that the first diffraction minimum occurs near $qa \approx 0.61$. (b) As for (a) but for partially absorbing walls ($\bar{\rho}a/D = 2$).

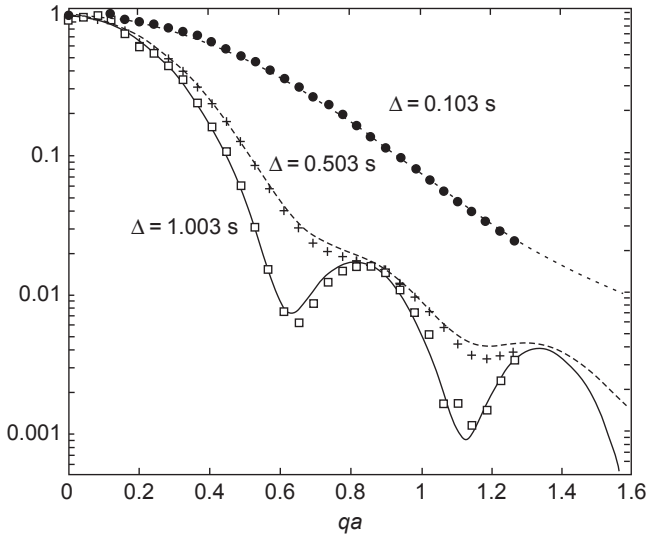

Fig. 7.11 Experimental data (points) and prediction of eqn 7.36 for pulsed field gradients applied orthogonal to the axis of a water-filled, 50 micron i.d. capillary, for three different diffusion times corresponding to $D\Delta/a^2 = 0.098$, 0.48, and 0.96. (Adapted from Gibbs [13].)

observed in the plane parallel pore, except that the echo minimum is at $qa/2\pi \approx 0.61$, and the first diffraction maximum occurs at an even greater degree of echo attenuation. Again, the effect of relaxation is to shift the diffraction minimum to higher q.

Equation 7.36 has been tested experimentally by S.J. Gibbs [13]. The theoretical lines, which correspond to $\bar{\rho} = 0$, are not fits, but predictions based on independently determined parameters. The agreement is very good, with residual deviations from the theory possibly due to non-orthogonality of the cylinder axis and the pulsed gradient direction.

7.2.4 Spherical pore

For the spherical case, the gradient of magnitude q is applied along the polar axis of the spherical polar coordinate frame. The relaxing boundary is at a radial distance $r = a$ from the sphere centre. The Helmholtz eigenmodes are

$$u_n(r,\theta,\phi) = \left\{ \begin{array}{c} j_n(\alpha_{nk} r) \\ h_n(\alpha_{nk} r) \end{array} \right\} \left\{ \begin{array}{c} P_n^l(\theta) \\ Q_n^l(\theta) \end{array} \right\} \left\{ \begin{array}{c} \cos(l\phi) \\ \sin(l\phi) \end{array} \right\} \tag{7.37}$$

where j_n and h_n are spherical Bessel functions of the first and second kind, and the P_n^l are associated Legendre functions. Since $h_n(\alpha_{nk} r)$ diverges as $r \to 0$, the $j_n(\alpha_{nk} r)$ solution is required for a spherical pore. Given azimuthal symmetry around the polar axis defined by that applied magnetic field gradient in the PGSE NMR experiment, only the $\cos(l\phi)$ solution with $l = 0$ is permitted, and P_n^l reduces to the Legendre polynomial P_n.

The eigenfunction expansion for the propagator is given by

$$\begin{aligned} P(\mathbf{r}|\mathbf{r}',\Delta) = \frac{1}{2\pi a^3} \sum_{n,k} \exp(-\frac{\alpha_{nk}^2 D\Delta}{a^2}) \frac{2n+1}{j_n^2(\alpha_{nk}) - j_{n-1}(\alpha_{nk}) j_{n+1}(\alpha_{nk})} \\ \times j_n(\alpha_{nk} r/a) j_n(\alpha_{nk} r'/a) P_n(\cos\theta) P_n(\cos\theta') \end{aligned} \tag{7.38}$$

where the j_n are spherical Bessel functions. The eigenvalues are determined by

$$\alpha_{nk} \frac{j_n'(\alpha_{nk})}{j_n(\alpha_{nk})} = -\frac{\bar{\rho} a}{D} \tag{7.39}$$

Noting that $\int_0^\pi P_n(\cos\theta) \exp(i2\pi qr\cos\theta) d(\cos\theta)$ is $2(-i)^n j_n(qr)$, and using the usual recurrence relations on spherical Bessel functions [15], it can be shown, after some algebra, that

$$\begin{aligned} E(q,\Delta) = \frac{3}{2} \sum_{n,k} \exp(-\frac{\alpha_{nk}^2 D\Delta}{a^2}) \frac{2n+1}{j_n^2(\alpha_{nk}) - j_{n-1}(\alpha_{nk}) j_{n+1}(\alpha_{nk})} \\ \{\alpha_{nk} j_n(qa)[j_{n-1}(\alpha_{nk}) - j_{n+1}(\alpha_{nk})] \\ \times \frac{-(qa) j_n(\alpha_{nk})[j_{n-1}(qa) - j_{n+1}(qa)]\}^2}{[(qa)^2 - \alpha_{nk}^2]^2} \end{aligned} \tag{7.40}$$

which reduces to the simpler form,

$$E(q,\Delta) = \sum_{n,k} 6\exp(-\frac{\alpha_{nk}^2 D\Delta}{a^2})\frac{(2n+1)\alpha_{nk}^2}{(\bar{\rho}a/D-\frac{1}{2})^2+\alpha_{nk}^2-(n+\frac{1}{2})^2} \times\frac{\{(qa)j_n'(qa)+(\bar{\rho}a/D)j_n(qa)\}^2}{[(qa)^2-\alpha_{nk}^2]^2} \tag{7.41}$$

Setting $q = 0$, eqn 7.41 reproduces the Brownstein–Tarr spherical pore result. Setting $\bar{\rho} = 0$ it encompasses the perfectly reflecting wall case derived by Balinov *et al.* [16].

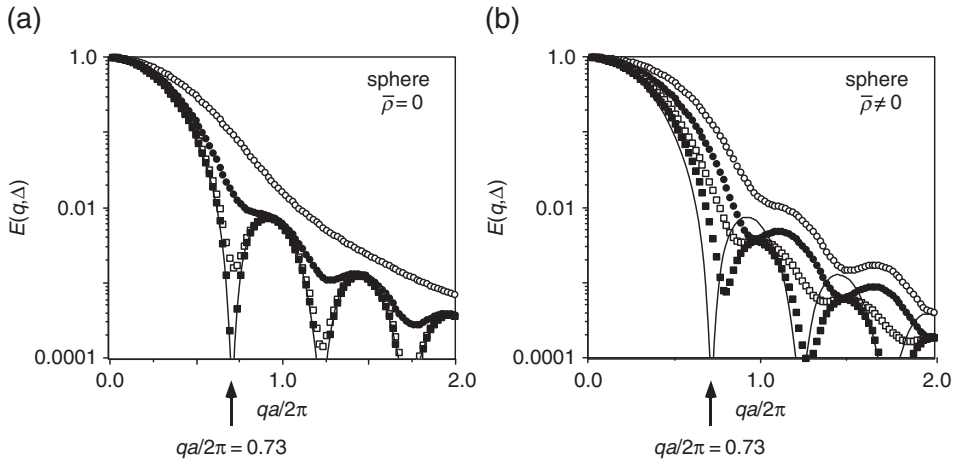

Fig. 7.12 (a) Echo attenuation, $E(q,\Delta)$, for spins trapped in a spherical pore of radius a and for perfectly reflecting walls ($\bar{\rho}a/D = 0$). Four successive time intervals are displayed. In multiples of a^2/D, Δ is, respectively, 0.2 (open circles), 0.5 (solid circles), 1.0 (open squares), and 2.0 (solid squares). Also shown is the theoretical curve for the infinite time diffraction pattern. Note that the first diffraction minimum occurs near $qa \approx 0.61$. (b) As for (a) but for partially absorbing walls ($\bar{\rho}a/D = 2$).

Figure 7.12 shows echo attenuations calculated using eqn 7.41 for a range of echo times both with and without wall relaxation. The phenomena are similar to those observed in the plane parallel and cylindrical pores, except that the echo minimum is at $qa/2\pi \approx 0.73$, and the first diffraction maximum occurs at $E(q,\Delta) < 0.01$. Figure 7.13 shows the absolute effect of relaxation on the unnormalised echo attenuation, while Fig. 7.12(b) shows the effect on the normalised attenuations.

In each of the geometries considered, the effect of wall relaxation is to shift the minima of the diffraction patterns to lower q values, thus making the pore size appear smaller. A similar effect is found even for non-relaxing walls when the duration of the gradient pulses becomes significant compared with the time to diffuse across the pore.

7.2.5 Finite width gradient pulses and relaxation effects

The apparent pore 'shrinking' evident in Figs 7.8, 7.10, and 7.12, as wall relaxation effects are included, is easy to understand. The 'spin-killing' in the vicinity of the wall

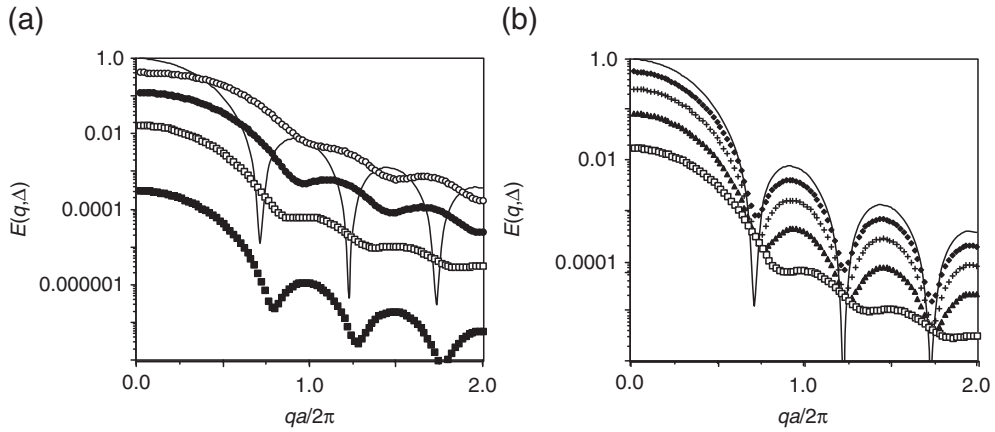

Fig. 7.13 (a) As for Fig. 7.12 (spherical pore case with $\bar{\rho}a/D = 2$) but with absolute rather than normalised echo amplitudes. Note that the diffraction minimum is strongly right shifted but moves closer to $qa/2\pi \approx 0.73$ at longer observation times. (b) Absolute echo attenuation for spins trapped in spherical pores of radius a at a fixed time $\Delta = a^2/D$ and for four different values of $\bar{\rho}a/D = 2$, namely 0.2 (solid diamonds, 0.5 (crosses), 1.0 (solid triangles), and 2.0 (open squares). Also shown for comparison is the theoretical curve for the infinite time diffraction pattern where $\bar{\rho} = 0$.

has the effect of reducing the local magnetisation density, causing a corona of reduced spin probability density in the vicinity of the wall. The immediate effect is to cause the apparent pore size, as viewed in the diffraction pattern, to reduce.

Careful inspection of Fig. 7.12(b) suggests a time-dependent shift in the position of the diffraction minimum for the spherical pore, an effect also observed more subtly in the cylindrical case. The reason is also easily understood. For the sphere, the relevant spin motion is parallel to the magnetic field gradient, which also defines the polar axis. At short times, reflection and relaxation of spins proximal to the wall will be dominated by the high proportion of molecules located at equatorial latitudes (near $\theta = 90°$), where the shorter chord lengths parallel to the polar axis make wall collisions more likely and the proportionate 'shrinking' of the apparent sphere diameter greater. At longer times, the repetitive relaxation suffered by such spins reduces their influence on the diffraction pattern, and the role of spins away from the equator increases. These shift phenomena indicate the need to account for both relaxation and finite observation time effects in analysing PGSE NMR data obtained for spherical pores.

Another 'pore shrinkage effect' results from the use of a finite duration gradient pulse in the PGSE NMR experiment. Impulse propagator matrix theory [18] can be used to predict the echo attenuation, and in the case of the plane parallel pore the results are shown in Fig. 7.14. These predictions agree precisely with independent Monte Carlo simulations [12, 14] and numerical solutions [17] to the Bloch–Torrey equation. It is apparent in Fig. 7.14 that the position of the first minimum in $E(q, \Delta)$ moves to higher values of q as the pulse duration is increased. This shift, which has been noted by a number of authors [12, 17, 19, 20], is, like the wall relaxation effect,

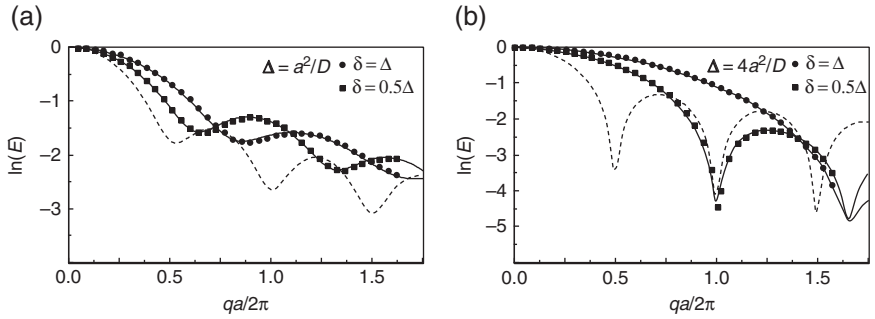

Fig. 7.14 Comparison of the impulse-propagator theory with numerical solutions to the magnetisation diffusion equation [17] for finite pulse-width PGSE attenuation in the case of restricted diffusion between parallel planes of spacing $2a$. No parameters have been adjusted and the comparison is absolute. The solid line shows the result calculated using the impulse propagator matrix theory [18], while the dashed curve shows the result predicted by the narrow gradient pulse approximation. (These data are adapted from reference [11] but with the plane spacing changed to $2a$ rather than the value of a used in that reference.)

associated with a narrowing in the effective well size by virtue of collisions of molecules with the boundaries. This narrowing was nicely explained by Mitra and Halperin [19] by invoking the 'smoothing' effect over the particle trajectory of the finite encoding time δ. Figure 7.15 illustrates how this results in the effective position of the particle during encoding being shifted out from the wall.

The probability distribution shown in Fig. 7.15(b) indicates a form of motional averaging that increases progressively as δ increases. Remarkably, Fig. 7.14 shows that the position of the first diffraction minimum continues to move to higher q as the diffusion length $D\Delta/a^2$ increases, with no asymptotic limit being evident.

7.3 Interconnected pores

While the simple 'diffusive-diffraction' long-time limit, $D\Delta/l_s^2 \rightarrow \infty$, may be achievable for an enclosing pore in which one length scale l_s describes the pore size, for interconnected pores, when multiple length scales exist, the diffractive limit breaks down, and the description is necessarily more complex. Of course, the eigenmode solution to the diffusion equation adopted in the previous section incorporates the finite displacements of molecules over an adjustable timescale and has diffusive-diffraction as a limiting case for long times. The same eigenmode approach can, in principle, be adopted for any enclosing geometry, including an array of interconnected pores, and where that geometry has some natural periodicity the general solution is quite practicable. For disordered structures, alternative strategies are required.

One means of making the problem tractable is to adopt a separation of timescales in which the diffractive limit applies at the length scale of the pore, while interpore diffusion spreads the diffraction pattern across a lattice of pores. This is known as the

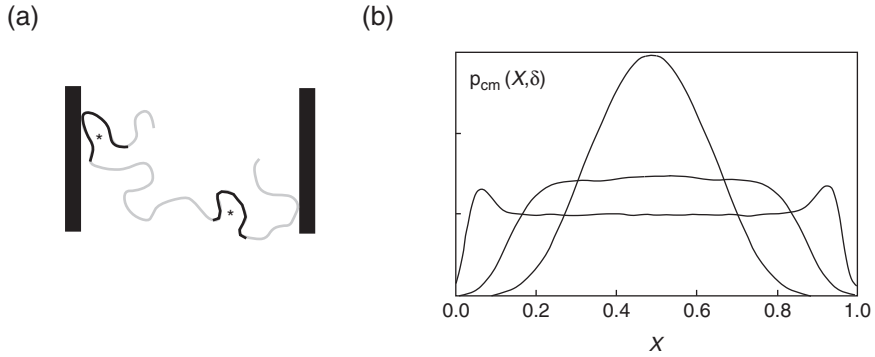

Fig. 7.15 (a) Trajectory of molecule diffusing between parallel plates with reflecting walls. The dark part of the trajectory corresponds to the periods δ when the gradient pulse is applied. The asterisks show the effective centre of mass of the particle during that pulse, and illustrate how collision with the wall necessarily shifts the centre of mass away from the wall. (b) Centre of mass distribution obtained by simulating molecules diffusing in a plane parallel pore ($2a = 1.0$) with reflecting walls. Note the narrowing as $\sqrt{D_0\delta} = 0.1$, 0.5, and 1. (Adapted from Mitra and Halperin [19].)

'pore equilibration assumption'. Within that assumption, two models are available to calculate the lattice contribution, one adopting a simple spreading Gaussian envelope of pore occupancy, and the other allowing, through a pore-hopping process, for the inter-pore diffusion to arise implicitly. Both give simple analytic expressions for the echo attenuation over a range of times longer than that required to diffuse across a single pore.

Note that material structures comprising an array of pores can be depicted as the convolution of a lattice with a pore density function. The Fourier space of such a material thus comprises a pore structure factor multiplied by a reciprocal lattice. This reciprocal lattice idea will be important in treating the problem of diffusion in an interconnected pore space.

7.3.1 Eigenmodes of the interconnected pore space

In the case of a porous medium with periodic microstructure, it is possible to adopt some of the methods used to describe the electronic properties of crystalline solids.[6] In particular the energy eigenfunctions (with energy eigenvalue $E_n = \hbar\omega_n$) for an electron in a periodic potential may be described by 'Bloch waves', products of a plane wave and functions that are periodic with the lattice potential, whence

$$\Psi_{n\mathbf{p}}(\mathbf{r}, t) = \phi_{n\mathbf{p}}(\mathbf{r}) \exp(i\mathbf{p} \cdot \mathbf{r} - i\omega_n t). \tag{7.42}$$

[6]The diffusion equation is similar to the Schrödinger equation for a moving particle but with an imaginary time. Consequently, solutions to the Schrodinger equation can form a nice starting point.

$\mathbf{p}$ is a wavevector in the first Brillouin zone[7] in reciprocal space and $\phi_{n\mathbf{p}}(\mathbf{r})$ is a function with the lattice periodicity. The eigenmode index n is said to label the 'band'. In this manner, Mitra *et al.* [9] suggested that the eigenmodes of the diffusion equation may be written in the form, $\phi_{n\mathbf{p}}(\mathbf{r})\exp(i\mathbf{p}\cdot\mathbf{r}-\lambda_{n\mathbf{p}}t)$, and using the Bloch–Floquet theorem, expanded $\phi_{n\mathbf{p}}(\mathbf{r})$ in a Fourier series of the reciprocal lattice vectors, $\mathbf{g}$, as

$$\phi_{n\mathbf{p}}(\mathbf{r}) = \sum_{\mathbf{g}} \tilde{\phi}_{n\mathbf{p}}(\mathbf{g})\exp(i\mathbf{g}\cdot\mathbf{r}) \tag{7.43}$$

where

$$\tilde{\phi}_{n\mathbf{p}}(\mathbf{g}) = \frac{1}{V_a}\int_{V_a} d\mathbf{r}\phi_{n\mathbf{p}}(\mathbf{r})\exp(-i\mathbf{g}\cdot\mathbf{r}) \tag{7.44}$$

and V_a is the volume of the unit cell.

It follows directly from eqns 1.47 and 1.52 that the periodic part of the diffusion eigenmode satisfies

$$\lambda_{n\mathbf{p}}\phi_{n\mathbf{p}} + D(\nabla + i\mathbf{p})^2\phi_{n\mathbf{p}} = 0 \tag{7.45}$$

and[8]

$$D\hat{\mathbf{n}}\cdot\nabla\phi_{n\mathbf{p}}(\mathbf{r}) + \bar{\rho}\phi_{n\mathbf{p}}(\mathbf{r}) = 0 \tag{7.46}$$

The diffusion propagator in the periodic medium can therefore be written

$$P(\mathbf{r}|\mathbf{r}',t) = \sum_{n\mathbf{p}} e^{-\lambda_{n\mathbf{p}}t}\phi_{n\mathbf{p}}(\mathbf{r})\phi_{n\mathbf{p}}(\mathbf{r}')e^{i\mathbf{p}\cdot(\mathbf{r}-\mathbf{r}')} \tag{7.47}$$

In principle, the echo-attenuation expression may be simply calculated by evaluating the expression

$$\begin{aligned} E(\mathbf{q},t) &= \int_{V_p} d\mathbf{r}\rho(\mathbf{r})\int_{V_p} d\mathbf{r}' P(\mathbf{r}|\mathbf{r}',t)\exp(i\mathbf{q}\cdot(\mathbf{r}'-\mathbf{r})) \\ &= \frac{1}{V_p}\int_{V_p} d\mathbf{r}\int_{V_p} d\mathbf{r}' P(\mathbf{r}|\mathbf{r}',t)\exp(i\mathbf{q}\cdot(\mathbf{r}'-\mathbf{r})) \end{aligned} \tag{7.48}$$

where V_p is the volume of the pore space and the fluid density is taken to be uniform.[9]

Because $\phi_{n\mathbf{p}}(\mathbf{r})$ is a function restricted to the pore space, solving the diffusion equation for any pore shape is not trivial. However, Bergman and Dunn [21–23] tackled this problem in an ingenious manner by treating it as the solution to a chemical-potential diffusion equation, which must be satisfied everywhere. They do this by defining a spatially dependent diffusion coefficient, $D(\mathbf{r})$, which vanishes in the solid matrix and is equal to the free diffusion value, D, outside, as well as by defining the characteristic or indicator function of the pore space, $\theta(\mathbf{r})$, which is 1 for $\mathbf{r}$ in the pore

[7]The first Brillouin zone is simply a Wigner–Seitz primitive cell of the reciprocal lattice of the periodic structure.

[8]$\mathbf{p} = 0$ at the boundary.

[9]Note that we here write $\mathbf{q}$ in angular frequency units, so as to match the convention for the momentum vectors of solid state physics. The $\mathbf{q}$ used here is equivalent to the $2\pi\mathbf{q}$ that applies when cyclic frequencies are used.

space and zero in the matrix. Restriction of $\phi_{n\mathbf{p}}(\mathbf{r})$ to the pore space implies that the relevant Fourier spectrum in terms of lattice vectors is

$$\theta(\mathbf{r})\phi_{n\mathbf{p}}(\mathbf{r}) = \sum_{\mathbf{g}} \tilde{\psi}_{n\mathbf{p}}(\mathbf{g}) \exp(i\mathbf{g}\cdot\mathbf{r}) \tag{7.49}$$

where

$$\tilde{\psi}_{n\mathbf{p}}(\mathbf{g}) = \frac{1}{V_a}\int_{V_a} d\mathbf{r}\theta_p(\mathbf{r})\phi_{n\mathbf{p}}(\mathbf{r}) \exp(-i\mathbf{g}\cdot\mathbf{r}) \tag{7.50}$$

The echo-attenuation function then becomes

$$\begin{aligned} E(\mathbf{q},t) = \frac{1}{V_p}\sum_{n,\mathbf{p}}\int_{V_p} d\mathbf{r}\sum_{\mathbf{g}}\tilde{\psi}_{n\mathbf{p}}(\mathbf{g})\exp(i(\mathbf{g}+\mathbf{p}-\mathbf{q})\cdot\mathbf{r}) \\ \times\int_{V_p} d\mathbf{r}'\sum_{\mathbf{g}}\tilde{\psi}^*_{n\mathbf{p}}(\mathbf{g})\exp(-i(\mathbf{g}+\mathbf{p}-\mathbf{q})\cdot\mathbf{r}')e^{-\lambda_{n\mathbf{p}}t} \end{aligned} \tag{7.51}$$

Since $\int d\mathbf{r}\exp(i\mathbf{k}\cdot\mathbf{r})$ is the Dirac delta function $\delta(\mathbf{k})$, the integrals require $\mathbf{p} = \mathbf{q} - \mathbf{g}$, which restricts $\mathbf{p}$ in the sum. Further, since $\mathbf{p}$ is in the first Brillouin zone, the only reciprocal space vector permitted is that closest to $\mathbf{q}$, and which is labelled $\mathbf{g}_\mathbf{q}$. $\mathbf{g}_\mathbf{q}$ is, in effect, the unique reciprocal lattice vector that returns $\mathbf{q}$ to the first Brillouin zone. In consequence, the echo-attenuation expression reduces to

$$E(\mathbf{q},t) = \frac{1}{\phi}\sum_{n} e^{-\lambda_{n\mathbf{p}}t}|\tilde{\psi}_{n\mathbf{p}}(\mathbf{g}_\mathbf{q})|^2 \tag{7.52}$$

where $\mathbf{p} = \mathbf{q} - \mathbf{g}_\mathbf{q}$.

Figure 7.16 shows a set of normalised echo-attenuation calculations, $E(\mathbf{q},t)/E(0,t)$, based on eqn 7.52, and calculated over a range of echo times, for a cubic array of overlapping spheres ($\phi = 0.202$) where the wall relaxivity is taken to be both zero and finite [24]. The gradient wavevector is aligned with the (100) direction, and the data exhibit the expected echo maximum corresponding to the Bragg peak at $qa/2\pi = 1$. The results agree remarkably well with simulations, and the diffraction patterns exhibit very little dependence on relaxation. In particular, we note that unlike the case of the isolated pore, where wall relaxation makes the pore appear smaller and hence the diffraction peak moves to larger q value, in the case of a periodic lattice the reciprocal lattice spacings are unaffected by relaxation and so the Bragg peak positions remain fixed.

Of course the periodic lattice model, while tractable analytically, is unlikely to be representative of most porous media where structural disorder, orientational and translational, will tend to dominate the behaviour. In the next section we outline the pore equilibration model whereby a tractable theory may be developed. However, the periodic lattice-Bloch eigenmode approach has an especially useful contribution to make in calculating the limiting behaviour of the effective diffusion as $t \to \infty$, yielding a result that may well have applicability in disordered systems. Of course the asymptotic limit will be associated with the echo-attenuation data as $q \to 0$, and

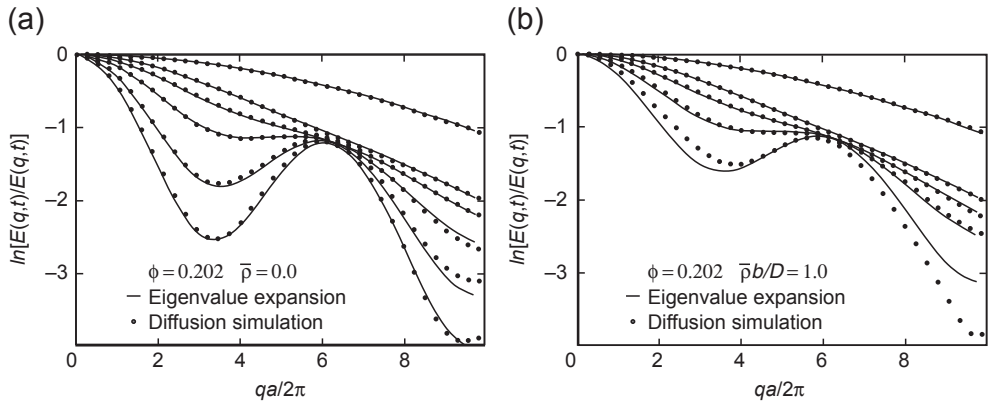

Fig. 7.16 Normalised echo attenuations obtained over a range of echo times for a porous medium consisting of a cubic array of overlapping spheres in (a) for $\bar{\rho}b/D = 0$ and (b) $\bar{\rho}b/D = 1$, where b is the side length of the cubic unit cell. In each case the eigenmode expansion based on Bloch modes agrees well with simulations. (Adapted from Bergman *et al.* [24].)

hence for $\mathbf{g_q} = 0$. For $t \gg b^2/D_0$ the lowest ($n = 0$) mode dominates, and reference to eqn 7.45 suggests that D_{eff} will depend on the curvature of the lowest energy band at the centre of the Brillouin zone [25]. Using this approach for a dilute array of spheres, Sen *et al.* [25] obtained $D_{\text{eff}}/D_0 = 2/(3-\phi)$, a result consistent with the known formation factor $1/F = 2\phi/(3-\phi)$ [26].

7.3.2 Pore equilibration model

Let us suppose that the porous medium may be described by an interconnected series of pores, as shown in Fig. 7.17. Each pore centred at $\mathbf{r}_{0i}$ has a normalised local fluid density function,[10] $\rho_{0i}(\mathbf{r}-\mathbf{r}_{0i})$, so that the density function, $\rho(\mathbf{r})$, of the array can be represented by a superposition of local structures,

$$\rho(\mathbf{r}) = \frac{1}{N}\sum_{i=1}^{N} \rho_{0i}(\mathbf{r}-\mathbf{r}_{0i}) \tag{7.53}$$

Now we will use the pore equilibration assumption to write the conditional probability that describes the diffusive displacement of any molecule starting in the ith pore. To do so, we require that the time taken to diffuse across a pore is much shorter than the time taken to diffuse between pores. This assumption permits us to assign some probability C_{ij} for diffusion to the jth pore, but allocates the molecule equal probability of being anywhere within the jth pore once it arrives. Hence

$$P_i(\mathbf{r}|\mathbf{r}',\Delta) = \sum_{j=1}^{N} C_{ij}\rho_{0j}(\mathbf{r}-\mathbf{r}_{0j}) \tag{7.54}$$

[10]This function could include associated local pore throats, but in effect we regard these throats primarily as obstacles which slow diffusion between pores.

The validity of pore equilibration depends on the assumption that in the time needed to diffuse to distant pores, the labelled particles will diffuse back and forth several times within those pores, which they partially occupy. In effect this means that as time advances, the occupancy of pores distant from the starting pore will increase, but the local density distributions will remain the same as in equilibrium, albeit with a smaller amplitude. In other words we shall be concerned with timescales that are longer than a^2/D_0, but finite on the scale b^2/D_p, where a is a measure of the pore size, b is the average pore spacing, and D_p is the interpore diffusion coefficient. Thus, pore equilibration requires $D_0 b^2/D_p a^2 \gg 1$.

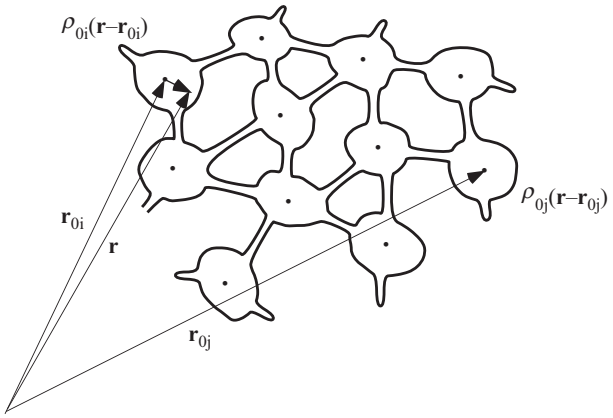

Fig. 7.17 Schematic representation of a general array of interconnected pores in which the local pore density functions are distributed on a lattice of points at locations $\mathbf{r}_{0i}$.

Pore equilibration: the Gaussian envelope

From eqn 7.54, we may write the echo attenuation when the gradient pulses are applied along the z-axis as

$$\begin{aligned} E(q,\Delta) &= \frac{1}{N}\sum_{i=1}^{N}\sum_{j=1}^{N} C_{ij}\int\int \rho_{0i}(z-z_{0i})\rho_{0j}(z-z_{0j}) \\ &\quad \times \exp(iq(z'-z_{0j}))\exp(-iq(z-z_{0i}))dz'dz \\ &\quad \times \exp(iq(z_{0j}-z_{0i}) \\ &= \frac{1}{N}\sum_{i=1}^{N}\sum_{j=1}^{N} C_{ij}\exp(iq(z_{0j}-z_{0i})S^{*}_{0i}(q)S_{0j}(q) \end{aligned} \tag{7.55}$$

If the pores are identical, then the product $S^{*}_{0i}(q)S_{0j}(q)$ is $|S_0(q)|^2$. For a structure with variable pore geometry we will define (somewhat roughly) an 'average pore structure factor', $\overline{|S_0(q)|^2}$ given by $\overline{S^{*}_{0i}(q)S_{0j}(q)}$. Thus

$$E(q,\Delta) = \overline{|S_0(q)|^2}\frac{1}{N}\sum_{i=1}^{N}\sum_{j=1}^{N} C_{ij}\exp\left(iq(z_{0j}-z_{0i})\right)$$
$$= \overline{|S_0(q)|^2}F(q,\Delta) \tag{7.56}$$

The connectivity matrix can now be applied to the problem of diffusion between the pores and the calculation of the lattice contribution to the echo attenuation, $F(q,\Delta)$. In the Gaussian envelope model the probability to be in neighbouring pores gradually increases according to a spreading diffusion profile written

$$C_{ij} = \frac{b}{(4\pi D_p\Delta)^{1/2}}\exp(-\frac{n_{ij}^2 b^2}{4D_p\Delta})$$
$$= \sum_i\{\sum_j \delta(Z-n_{ij}b)\}\otimes(4\pi D_p\Delta)^{1/2}\exp(-Z^2/4D_p\Delta) \tag{7.57}$$

where n_{ij} is a real number describing the fraction of lattice separations, b, that separate pores i and j. Thus $F(q,\Delta)$ involves a convolution between a 'lattice correlation function', $L(Z) = \sum_i\{\sum_j \delta(Z-n_{ij}b)\}$, and a diffusive envelope, $d(Z,\Delta) = (4\pi D_p\Delta)^{1/2}\exp(-Z^2/4D_p\Delta)$. For a regular periodic lattice with the gradient aligned along a crystallographic axis, n_{ij} will be a simple integer. For an irregular lattice or pore glass, we could replace $\sum_i\{\sum_j \delta(Z-n_{ij}b)$ by some general averaged lattice correlation function $\overline{L(Z)}$ and write the equation

$$E(q,\Delta) = \overline{|S_0(q)|^2}\left[\mathcal{F}\{d(Z,\delta)\}\otimes\mathcal{F}\{\overline{L(Z)}\}\right] \tag{7.58}$$

To evaluate this expression we need some suitable description of $\overline{L(Z)}$.

Figure 7.18 shows three examples of a perfectly regular lattice, a regular lattice with irregular spacing,[11] and a pore glass with irregular spacing. A practical description of the the irregular lattice correlation function, $\overline{L}(Z)$, is given by presuming a mean pore spacing b with standard deviation (on a Gaussian distribution) ζ. A molecule starting in one pore and moving to the next will find its position at a distance b with standard deviation ζ, but the next nearest neighbour at $2b$ will have standard deviation 2ζ and so on, the lattice correlation being gradually lost, as shown in Fig. 7.18. In this sense ζ is a correlation length, which defines the distance over which regularity in the lattice displacements decays.

For molecules migrating from a starting pore to neighbouring pores in a pore glass, the vectors describing the set of possible displacements will have some mean length b but no orientational regularity. Averaged over the entire sample we could consider the first neighbour set to be uniformly distributed on a surrounding spherical shell of radius b. To predict the outcome of the PGSE experiment, we require the distribution of projected distances, Z, resulting from diffusion to the nearest neighbour. A simple

[11] The case of regular periodic lattices is covered in detail in the author's earlier book, reference [27].

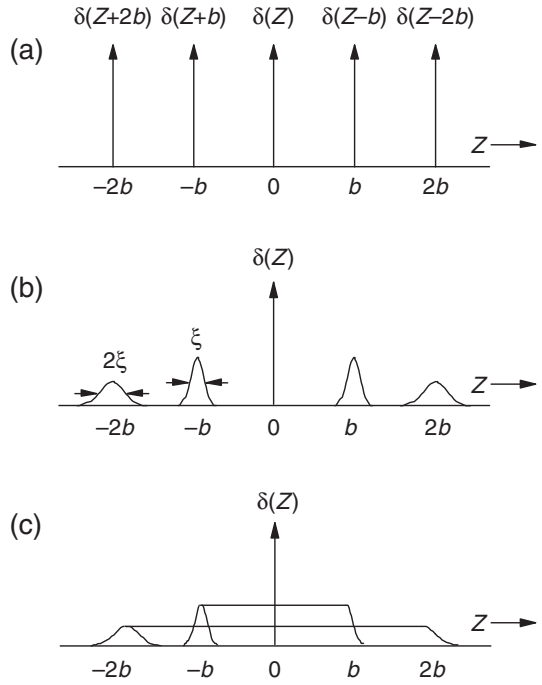

Fig. 7.18 The lattice correlation functions, $\overline{L(Z)}$, for (a) a regular 1-D lattice; (b) an irregularly-spaced 1-D lattice; (c) a pore glass. In (b) the Gaussians at each lattice site are successively broader for each pore successively displaced from the starting pore, with $\overline{L(Z)}$ becoming constant for $Z \gg b$. In (c) the pore glass lattice correlation function is a sum of normalised rectangular densities at each successive pore shell, convoluted with successively broader Gaussian pore separation distributions.

analysis shows that this probability density along Z is uniform for $-b < Z < b$, with magnitude $(2b)^{-1}$, and zero outside. For migration to the nth pore shell, the density is $(2nb)^{-1}$ between $-nb$ and nb. Thus, for the pore glass, $\overline{L(Z)}$ is a sum of hat functions of increasing width and decreasing height (conserving probability) associated with successive further neighbour pore shells, convolved with a Gaussian spread of increasing standard deviation $n\zeta$, and described by $(2\pi\zeta^2)^{-1/2}\exp(-Z^2/2n^2\zeta^2)$. Hence, the echo attenuation becomes

$$E(q,\Delta) = \overline{|S_0(q)|^2}\sum_n C_n \frac{\sin(qnb)}{qnb}\exp(-\tfrac{1}{2}q^2n^2\zeta^2) \tag{7.59}$$

where

$$C_n = 4\pi(nb)^2\frac{b}{(4\pi D_p\Delta)^{3/2}}\exp(-\frac{n^2b^2}{4D_p\Delta}) \tag{7.60}$$

Pore equilibration-the pore hopping model

The need to assume a Gaussian envelope for diffusive occupancy of the pore lattice can be avoided using a simple trick [28]. Suppose that we consider a time interval, τ,

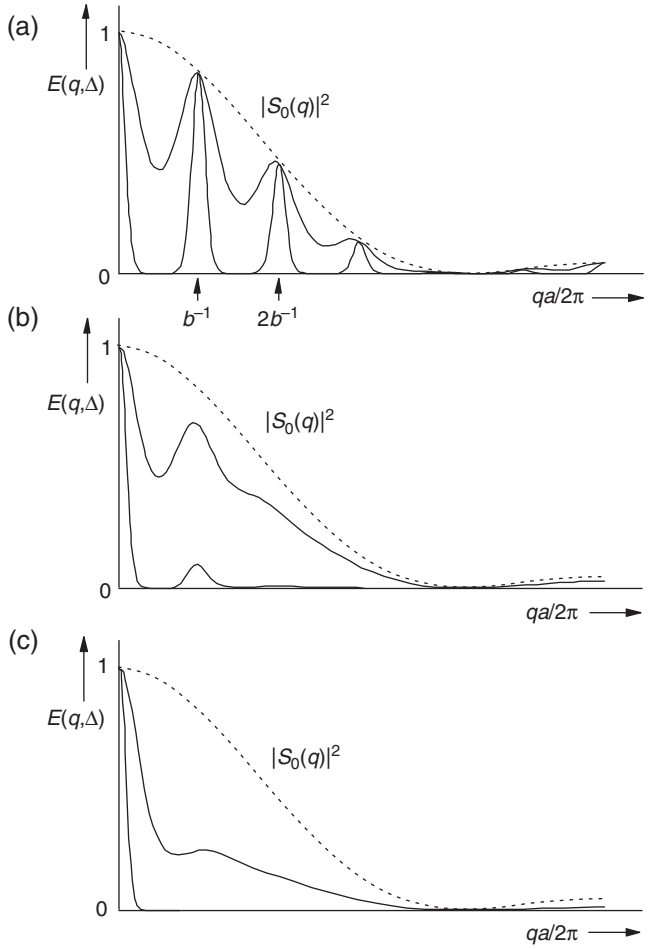

Fig. 7.19 $E(q, \Delta)$ vs q calculated using eqn 7.58: (a) regular lattice, (b) irregular 1-D lattice where $\xi = 0.2b$, and (c) irregular pore glass where $\xi = 0.2b$. In each case the pore is treated as a sphere with radius a approximately $b/3$ and $E(q, \Delta)$ is shown for Δ values of $0.2b^2/D_p$ and $2b^2/D_p$.

sufficiently short that molecules are most unlikely to have diffused further than the nearest pore. The resulting probability density function, $C(Z, \tau)$, involves only the starting pore and the nearest neighbour, and is easily written down exactly. Then, to calculate the pore hopping probability density for a finite time, $\Delta = M\tau$, all we need do is simply convolve $C(Z, \tau)$ M times so that

$$C(Z, \Delta) = C(Z, \tau) \otimes C(Z, \tau) \otimes \ldots .]_{M\ times} \tag{7.61}$$

The contribution, $F(q, \Delta)$ of pore hopping to the echo-attenuation function is therefore

$$\begin{aligned} F(q,\Delta) &= \mathcal{F}\{C(Z,\Delta)\} \\ &= \mathcal{F}\{[C(Z,\tau) \otimes C(Z,\tau) \otimes \ldots.]_{M\ times}\} \\ &= [\mathcal{F}\{C(Z,\tau)\}]^M \end{aligned} \tag{7.62}$$

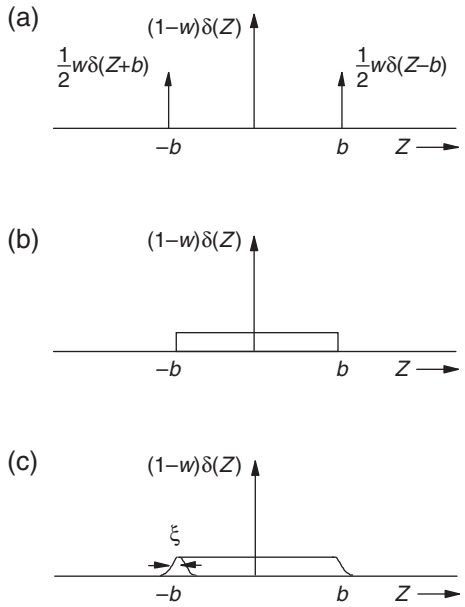

Fig. 7.20 Probability density functions, $C(Z,\tau)$, for hopping in an infinitesimal time interval τ, for (a) regular lattice, (b) pore glass with uniform pore spacing, (c) pore glass with irregular pore spacing. (Adapted from reference [28].)

Figure 7.20 shows $C(Z,\tau)$ for both a regular lattice and a pore glass, where we assume that the hopping probability in time τ is w. They may be written as:
(a) regular lattice

$$C(Z,\tau) = (1-w)\delta(Z) + \tfrac{1}{2}w[\delta(Z-b) + \delta(Z+b)] \tag{7.63}$$

(b) regularly spaced pore glass

$$C(Z,\tau) = (1-w)\delta(Z) + \frac{w}{2b}[H(Z-b) - H(Z+b)] \tag{7.64}$$

(c) irregularly spaced pore glass

$$\begin{aligned} C(Z,\tau) = (1-w)\delta(Z) + \frac{w}{2b}[H(Z-b) - H(Z+b)] \\ \otimes (2\pi\zeta^2)^{-1/2} \exp(-Z^2/2\zeta^2) \end{aligned} \tag{7.65}$$

where H represents the Heaviside step function.

One more step is needed before the final echo attenuation expressions can be calculated, and that is to relate w and b to the interpore diffusion coefficient, D_p. To do so, we consider the low q limiting behaviour of the echo attenuation $E(q,\Delta) = |S_0(q)|^2 F(q,\Delta)$, thus emphasising the long-range displacements associated with the pore hopping. Of course the low q limit of $E(q,\Delta)$ becomes $1 - 4\pi^2 q^2 \langle Z^2(\Delta)\rangle$. In consequence, noting $|S_0(q)|^2 \to 1$ as $q \to 0$,

$$\begin{aligned}\langle Z^2(\Delta)\rangle &= -F''(q=0, M\tau) \\ &= Mwb^2 \\ &= 2D_p\Delta \end{aligned} \tag{7.66}$$

where the double prime denotes the second derivative with respect to q. Hence, we can identify

$$w = \frac{2D_p\Delta}{Mb^2} \tag{7.67}$$

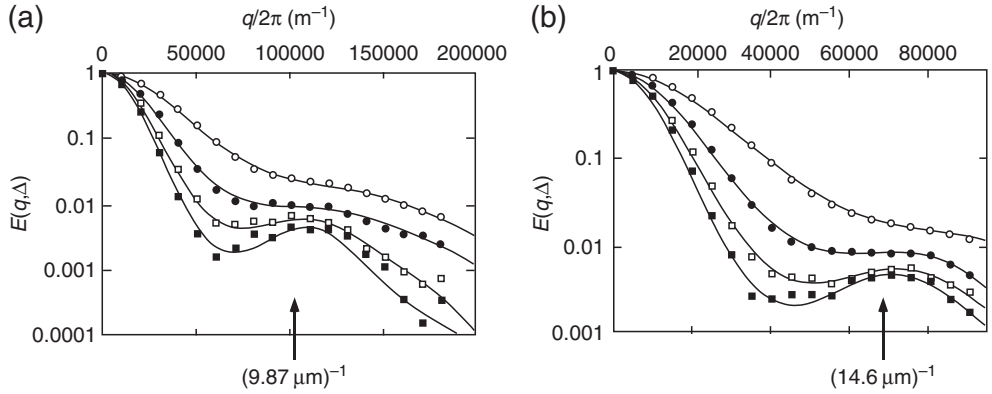

Fig. 7.21 Echo-attenuation functions, $E(q,\Delta)$, resulting from the diffusion of water in a bed of randomly packed monodisperse polystyrene spheres of diameter (a) 9.87 microns and (b) 14.6 microns, where the observation times, Δ, range from 10 ms (open circles), 20 ms (closed circles) 30 ms (open squares) to 40 ms (closed squares). The solid lines are fits using eqn 7.70. (Adapted from reference [29].) Note the coherence peak at $q/2\pi \sim b^{-1}$ where the pore spacing b is comparable to the bead diameter.

Evaluating the Fourier spectrum of $C(Z,\tau)$ in each of the cases given in eqns 7.63, 7.64, and 7.65, and taking the Mth power we find:
(a) regular lattice

$$E(q,\Delta) = |S_0(q)|^2 \exp\left(-\frac{4D_p\Delta}{b^2}\sin^2(\tfrac{1}{2}qb)\right) \tag{7.68}$$

(b) regularly spaced pore glass

$$E(q,\Delta) = |S_0(q)|^2 \exp\left(-\frac{6D_p\Delta}{b^2}\left[1 - \frac{\sin(qb)}{qb}\right]\right) \tag{7.69}$$

(c) irregularly spaced pore glass

$$E(q,\Delta) = |S_0(q)|^2 \exp\left(-\frac{6D_p\Delta}{b^2+3\zeta^2}\left[1-\exp(-\tfrac{1}{2}q^2\zeta^2)\frac{\sin(qb)}{qb}\right]\right) \tag{7.70}$$

Figure 7.21 shows the results of PGSE NMR echo attenuation experiments [29] carried out on water diffusing in a porous medium consisting of a pore glass made from randomly packed monodisperse polystyrene spheres with nominal diameters 9.87 microns and 14.6 microns. In each case a coherence peak is clearly visible at $q/2\pi \sim b^{-1}$, the pore spacing, b, being on the order of a bead diameter. Note that the amplitude of this peak is at an attenuation value $E(q,\Delta) < 0.01$, thus placing demands on experimental signal-to-noise ratio. In each case the data are fitted using eqn 7.70, assuming a somewhat simplistic spherical pore shape, radius a. The representation of the data is good, with reasonably consistent parameter values. For example, in the case of the 9.87 micron spheres, of $a \sim 3\ \mu$m, $\xi \sim 2\ \mu$m, $D_p \sim 2x10^{-9}$ m^2 s^{-1}, and with b ranging from $6.2\,\mu$m to $10.6\,\mu$m with increasing Δ. That the fitted pore spacing should depend on observation time is perhaps not surprising given the simplicity of the underlying pore equilibration assumption. Equations 7.68, 7.69, and 7.70 are certainly not exact, but they do provide insight and are a conveniently simple representation of the restricted diffusion process in interconnected porous media.

7.3.3 'Long-narrow' PGSE NMR and interconnected pores

While the long-narrow PGSE NMR approach provides an obvious advantage in diffraction studies of enclosing pores, in the case of interconnected pores the method suffers from a significant disadvantage. Over the long gradient pulse, molecules will diffuse from pore to pore, at an asymptotic diffusion rate given by D_p. The final narrow gradient pulse will return the spectrum $S_0(q)$, as a coefficient in the echo attenuation, provided that the duration of that pulse is much shorter than the time to diffuse across a pore. But this structure factor will be multiplied (in the pore equilibration picture) by a factor relating to the inter-pore diffusion, and, because the inter-pore length distances will generally exceed the pore dimension, the damping factor may be so great as to mask the spectrum.

Of course, it could be argued that the narrow-pulse PGSE NMR method also returns a structure factor (in this case the less information-rich $|S_0(q)|^2$) experiencing a similar damping due to inter-pore diffusion, as evident in eqn 7.58. But now we see a crucial difference between the methods. For narrow pulse PGSE NMR, one is sensitive to inter-pore diffraction effects, in addition to pore-scale diffraction. Indeed, as eqn 7.58 makes clear, inter-pore diffraction dominates the echo attenuation, the term $|S_0(q)|^2$ merely providing a weakly decaying envelope. Alas, inter-pore diffraction cannot be observed in long-narrow PGSE NMR because, in trading the short initial gradient pulse for a long weak pulse, we have gained the pore structure factor directly, but lost the interference effects associated with migration across the pore lattice, accepting in return a gaussian decay associated with inter-pore diffusion in the presence of a weak steady gradient.

In the spirit of eqn 7.25, we may write down the echo attenuation for the interconnected pore space signal of the long-narrow PGSE NMR method as

$$\begin{aligned} E(q,T) &= \big\langle \exp\big(-iq\frac{1}{T}\int_0^T z_p(t)dt\big)\big\rangle\overline{S_0(q)} \\ &= \exp(-\tfrac{1}{3}q^2D_pT)\overline{S_0(q)} \end{aligned} \tag{7.71}$$

It may be possible, for sufficiently small inter-pore diffusion time T, that the diffusive prefactor $\exp(-\frac{1}{3}q^2D_pT)$ does not overwhelm the averaged pore structure factor $\overline{S_0(q)}$, making pore size characterisation feasible.[12] In that case, having measured the non-asymptotic D_p value applicable to the chosen value of T, the factor $\exp(-\frac{1}{3}q^2D_pT)$ can be calculated for each q value, and normalised out, leaving $\overline{S_0(q)}$ directly visible. At the time of writing of this book, that experimental possibility remains an, as yet, unproven possibility.

7.4 Applications of q-space diffraction

7.4.1 Emulsions and capsules

While it is possible to manufacture almost ideal plane parallel pores and cylindrical pipes of highly uniform spacing or radius, in the case of synthetic spherical particles, other factors intervene to complicate the q-space diffraction measurement. An obvious application of diffusive diffraction is in the analysis of the diffusive behaviour of molecules trapped inside spherical colloidal particles. Of course, the signal response will be complicated by the fact that the internal restricted diffusion will be superposed on the diffusion of the particle itself. What that means in effect is that the propagator for internal motion is convolved with the Gaussian propagator associated with the diffusion of the sphere. Provided that sphere radius a exceeds the length scale for sphere diffusion over the time $\Delta \gg a^2/D_0$, then diffusive diffraction effects will dominate. But even outside this condition the behaviours are inherently separable. Of course, inter-sphere diffusion (migration of molecules between spheres) and sphere radius polydispersity will further complicate or 'smear' diffusive diffraction effects. Nonetheless, such factors are are exactly analytically describable [30], and their convolution to generate the propagator that characterises the resultant molecular translational dynamics may be written down.

Examples of spherical colloidal particle systems include emulsions, core-shell particles, multi-lamellar onion phases, and polyelectrolyte multi-layer capsules. For emulsions, size polydispersity and inter-droplet diffusion certainly play an important role in determining the PGSE NMR signal response. Haakanson *et al.* have shown that in close-packed emulsions, it is possible to use diffraction effects resulting from inter-droplet migration to determine the local emulsion packing structure [31]. Wassenius *et al.* [32] have investigated the echo signal from molecules inside 'core-shell' latex particles with a liquid core of hexadecane and a solid polystyrene shell. At echo times long compared with that required to diffuse across the sphere, they found the root mean

[12]It is worth noting, however, that $\overline{S_0(q)}$ decays, with increasing q, at a much slower rate than $\overline{|S_0(q)|^2}$, making it more resilient to measurement in the face of inter-pore diffusive decay.

square displacement of oil inside the particle core to be constant for all diffusion times and, from that, calculated the mean particle radius. While the diffusive diffraction pattern in the echo decay was almost completely smeared out due to polydispersity and wall relaxation effects, a small 'bump' in $E(q)$ was observed at $qa \approx 0.7$. Yadav and Price [33] have seen both intra-sphere and inter-sphere diffraction effects from PGSE NMR experiments on water-in-oil emulsions, carrying out a detailed fit to the data using the multiple-propagator matrix method to allow for the influence of finite-width gradient pulse effects.

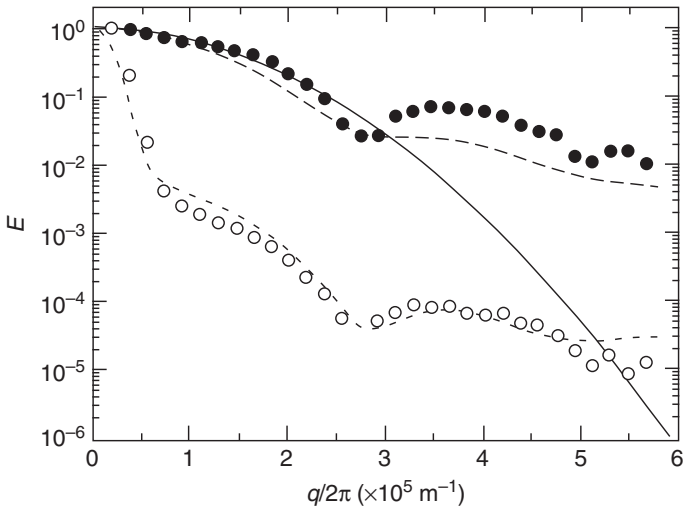

Fig. 7.22 $E(q, \Delta)$ vs q for both water (open circles) and tetramethyl ammonium chloride (TMA; closed circles) for a water/TMA in heptane emulsion. Here $\delta = 0.8ms$ and $\Delta = 0.5s$, while g is incremented from 0 to 17.2 T/m. The solid line is a fit using the Gaussian phase approximation model, while the dashed lines are multiple propagator diffraction fits. Note that inter-droplet effects are indicated for the water, but not the TMA signal. (Redrawn from Yadav and Price [33].)

Their echo-attenuation data, obtained from both water and tetramethyl ammonium chloride, are shown in Fig. 7.22 along with theoretical estimates. A simple Gaussian phase approximation model fails badly, as can be seen in Fig. 7.22, while the diffusive diffraction model works well when a distribution of sphere sizes is incorporated.

7.4.2 Biology and medicine

Ironically, monodispersity is more often observed in nature than achieved in synthesis. A remarkable example of distinctive size monodispersity in colloids is the mammalian blood cell. Kuchel and co workers [34–39] have carried out extensive studies of the size, shape, and permeability of human blood cells using PGSE NMR diffusive diffraction effects. This work has not only shown that erythrocytes orient in a magnetic field, but accurate shape and size determinations have been made using diffusive diffraction, and

shape evolution through various forms has been observed on poisoning with sodium fluoride.

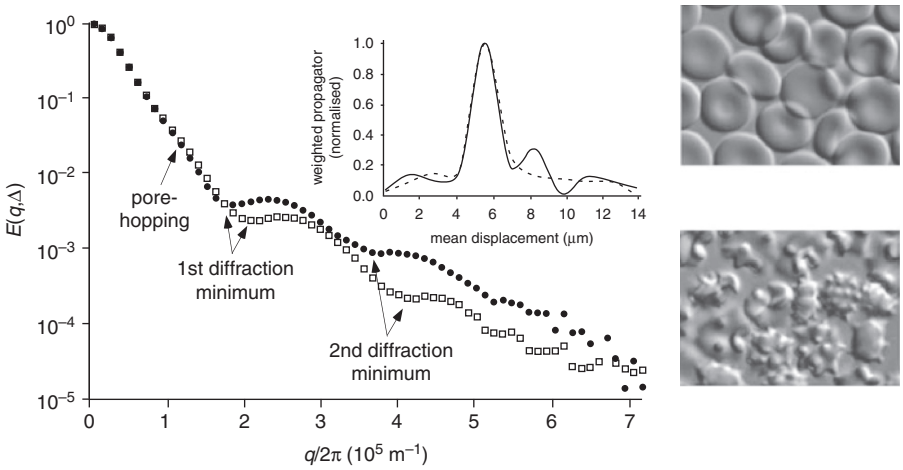

Fig. 7.23 $E(q, \Delta)$ vs q for red blood cell samples showing the influence of shape. The signals were obtained from predominantly discocytes (squares) and spherocytes (closed circles). The insets show the displacement distributions for both graphs. Discocyte and spherocyte microscope images are shown on the right of the figure. (Reproduced with permission from Pages *et al.* [39].)

An example of these data are shown in Fig. 7.23, where distinctly different diffraction patterns are obtained subsequent to introduction of the NaF. Also shown are size distributions based on a second-derivative method described in reference [38]. Note that at low q the inflection labelled 'pore-hopping' is due to diffraction effects related to water moving between cells. Using these methods Kuchel and co-workers have been able to monitor shape changes in erythrocytes over many hours.

7.4.3 Pulsed gradient spin-echo ESR

Given the short T_2 so common in electron paramagnetic resonance,[13] typically on the order of or short than $1\,\mu$s, the duration of gradient pulses in any possible PGSE time-domain ESR experiment will be similarly constrained to sub-microsecond. In addition, the short T_1, again typically on the order of or shorter than 1 μs, confines Δ to on the order of microseconds. Despite the larger gyromagnetic ratio of the electron spin, a pulsed gradient of $10\,\mathrm{T\ m^{-1}}$, at the high end of the experimentally feasible, would only allow the measurement of diffusion coefficients faster than $10^{-7}\,\mathrm{m^2\ s^{-1}}$, much faster than molecules in the liquid state, except at highly elevated temperatures.

[13]Also known as electron spin resonance or ESR.

There do, however, exist 'pathological' EPR samples with long relaxation times, one of the most notable being the 1-D organic metal (fluoroanthene)$_2$PF$_6$ [40], for which $T_1 \approx T_2 \approx 10\,\mu$s. Steady gradient diffusion methods have indicated [40, 41] that the upper limit for electron diffusion perpendicular to the conducting channels is at least three orders of magnitude smaller than in the longitudinal direction. In 1994 a PGSE ESR experiment [42] was performed on this system, in which both Δ and q (parallel to the longitudinal axis) were varied. The results were consistent with restricted diffusion in a one-dimensional well [43].

The switching of gradient pulses with duration on the order of $1\,\mu$s is difficult, even with gradient coils designed specifically for low inductance. The switching time achieved with conventional commercial linear current amplifiers is around $20\,\mu$s and limited by feedback loop circuitry. Overcoming this limitation is feasible using the 'clipped L-C resonance' idea of Conradi *et al.* [44] in which driven, semi-sinusoidal current pulses are generated. This method allows current pulses of any duration, δ, down to 2 μs, resulting in peak field gradients up to 1.0 T m^{-1} using a quadrupolar gradient coil of 0.2 T m^{-1}A^{-1} [42].

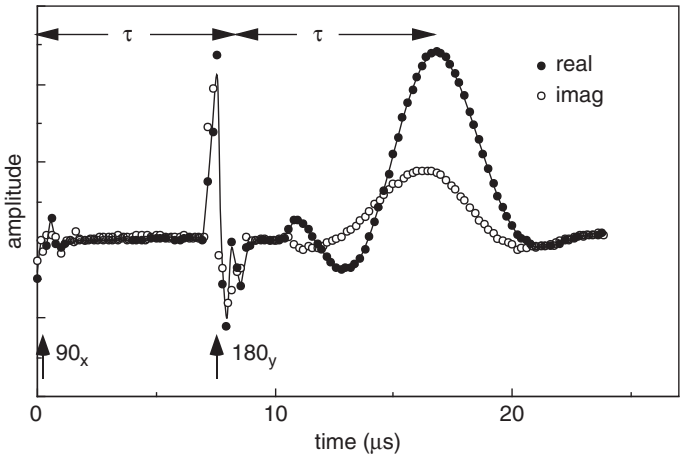

Fig. 7.24 Real and imaginary echo signals from a $90_x - \tau - 180_y$ spin-echo sequence ($\tau = 7.8\,\mu$s) after signal averaging from 1024 transients. The acquisition begins $0.5\,\mu$s before the first RF pulse although the correct phase cycling for signal co-addition does not begin until $0.5\,\mu$s following the second pulse. The additional delay before the signal appears is due to the $4\,\mu$s deadtime. (Reproduced with permission from reference [42].)

Figure 7.24 shows an example of an echo signal obtained from the electrons in the (fluoroanthene)$_2$PF$_6$ sample, obtained at 300 MHz using $B_0 = 10.5$ mT in the stray field region of a 7 T superconducting magnet [42]. The RF pulses were $0.2\,\mu$s and $0.4\,\mu$s, respectively, for the 90 and 180 degree RF pulses and were generated using a Bruker AMX300 NMR spectrometer. The echo shown was obtained with 1000 transients at $2\tau = 16\,\mu$s and at a repetition time of 2 ms, limited by the spectrometer data transfer rate rather than the sample T_1. Remarkably, the response of the echo amplitude to q

and Δ is consistent with restricted electron diffusion, in which the size, l, of the 1-D compartments is governed by an exponential distribution

$$p(l) = l\bar{l}^{-2} \exp(-l/\bar{l}) \tag{7.72}$$

associated with random defects. Using this length distribution, the planar restricted diffusion expression of eqn 7.30 provides a good fit to the data, as shown in Fig. 7.25.

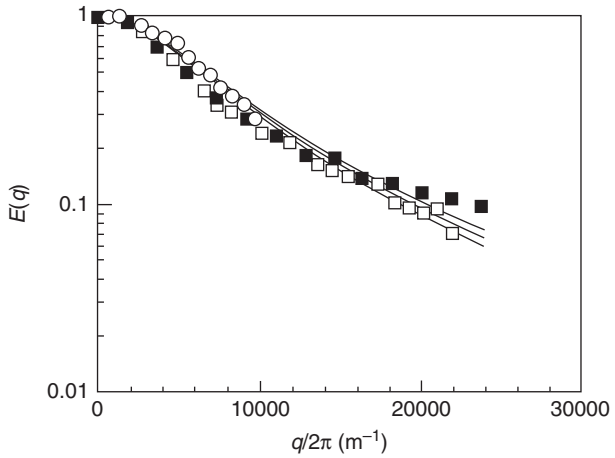

Fig. 7.25 Normalised echo-attenuation data for PGSE ESR from electrons in (fluoroanthene)$_2$PF$_6$ sample, corresponding to different Δ and δ values of (open circles) 14 μs and 2 μs, (closed squares) 16.5 μs and 2.6 μs, and (open squares) 19.5 μs and 2.6 μs, along with three curves representing best fits to the impenetrable relaxing wall model where $D = 1.8 \times 10^{-4}$ m^2 s^{-1}, $\bar{l} = 47\,\mu$m, and $\overline{\rho} = 0.01$. (Reproduced by permission from reference [43].)

7.5 Flow diffraction

The diffraction pattern shown in Fig. 7.1 arises because diffusing water molecules migrate from pore to pore in the beadpack, thus embedding in the displacement propagator features characteristic of the inter-pore geometry. In particular there exists a higher probability of displacement at distances corresponding to the pore spacing d, thus leading to the characteristic Bragg peak at $q/2\pi \sim 1/d$.

Of course diffusion merely provides the transport mechanism whereby the pore space is interrogated. It is equally possible to use advection. Such 'flow diffraction' effects were first observed for a system comprising a monodisperse packing of 90.7 micron diameter polystyrene spheres in deionised water. Just as the optimal time for observation of coherence via Brownian motion is $\Delta \sim b^2/D_{\text{eff}}$, so the optimal evolution time for flow coherence is $b/ < v >$. Note that for this system the Brownian time is around 4 s, a time at which magnetic relaxation completely destroys the signal. Hence the flow method provides a means of examining much larger pore spacings, in

the present case giving an optimal diffraction for a conveniently chosen $\Delta = 30\,\text{ms}$ when $< v >= 3.3\,\text{mm s}^{-1}$. Results for the echo-attenuation function $E(q)$are shown in Fig. 7.26, where the coherence peak due to displacement correlation of nuclei over the pore spacing is clearly evident as velocity is increased. Note the convenient control in this type of measurement, as increasing the velocity results in an increased length scale in the sampling of the pore spaces displaced from the starting pore.

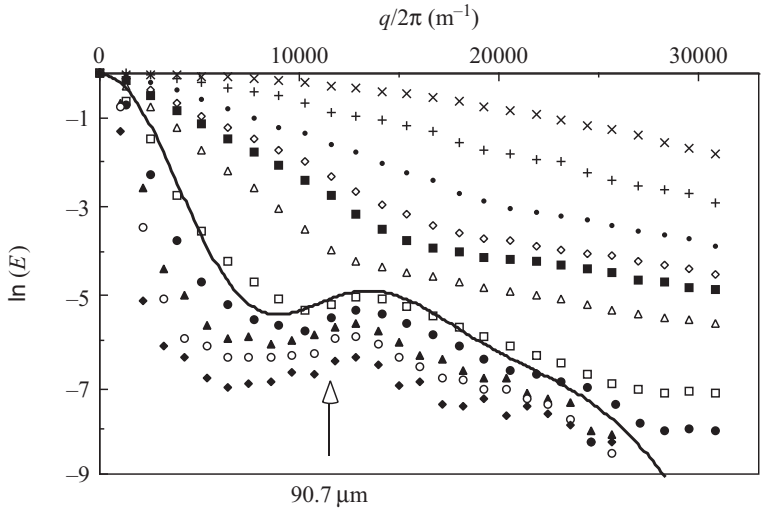

Fig. 7.26 $E(q)$ vs q for water flowing in a 90.7-micron diameter bead pack in which the magnetic field gradient is applied along the axial flow direction. Here $\Delta = 30\,\text{ms}$ and a coherence peak is evident for velocities corresponding to $\Delta > b/ < v >$. The data shown range from 0 to 8.7 mm/s. The line is a fit of eqn 7.70 to the 3.3 mm/s data (open squares). (Reproduced from reference [45].)

One set of data, corresponding to a mean flow rate of $< v >= 3.3\,\text{mm/s}$, is fitted in Fig. 7.26, using the diffusive diffraction pore hopping relation, eqn 7.70. In this case D_{eff} corresponds to the longitudinal dispersion coefficient obtained from the low-q limit of the data. The resulting parameters are $b = 82.5\,\mu\text{m}$, $a = 22.4\,\mu\text{m}$, and $\xi = 12.2\,\mu\text{m}$, quite reasonable estimates given the known bead diameter.

7.6 Related issues

7.6.1 Frequency-domain modulated gradient NMR and diffusive diffraction

An interesting question, which has generated a number of articles [46–49], concerns the ability of FDMG NMR experiments to be sensitive to diffusive diffraction effects. Recall that the mode of operation is typically a CPMG echo train, interspersed with gradient pulses or carried out in the presence of a constant magnetic field gradient. In order to clearly define the frequency, the echo train comprises many periods, each involving a small attenuation effect, which gradually accumulates with period number.

The method is effectively a manifestation of the central limit theorem in action, each period representing a low-q perturbation in which the Gaussian approximation applies, the cumulative effect of many Gaussians being ultimately a Gaussian echo train decay. Of course the Gaussian phase case can never embody coherence effects, and no such effects have been seen in these experiments.

The positive side of this ledger is that the cumulant truncation that underpins the interpretation of FDMG NMR is soundly based. And of course, there are good theories available for restricted diffusion under the Gaussian phase approximation, those of Robertson [50] and Neuman [51] being early examples. Kuchel *et al.* [52] have considerably extended this work, carrying out detailed calculations and numerical simulations of restricted diffusive effects in spheres with relaxing walls, under the GPA.

7.6.2 Return to origin probability

The narrow gradient pulse PGSE NMR experiments provide a means of accessing information about the probability that spin-bearing molecules displace a characteristic distance over a clearly defined diffusion time $t = \Delta$. One particularly interesting probability, $P_{RTO}(t)$, concerns the return of particles to origin, since through its time dependence we might gain some insight regarding pore space restrictions and connectivity [53, 54]. The measurement of $P_{RTO}(t)$ follows directly from the definition of the narrow gradient pulse echo attenuation, in eqn 5.81. Integrating each side of this equation we have

$$\begin{aligned}\int E(\mathbf{q},t)d\mathbf{q} &= \int \rho(\mathbf{r}) \int P(\mathbf{r}|\mathbf{r}',t) \left[\int \exp(i\mathbf{q}\cdot[\mathbf{r}'-\mathbf{r}])d\mathbf{q}\right] d\mathbf{r}'d\mathbf{r} \\ &= \int \rho(\mathbf{r})P(\mathbf{r}|\mathbf{r},t)d\mathbf{r} \\ &= \overline{P}(0,t) \end{aligned} \tag{7.73}$$

where $P_{RTO}(t) = \overline{P}(0,t)$ is the average propagator in the case $\mathbf{R} = 0$. The return to origin probability is thereby obtained by integrating the normalised echo attenuation over all $\mathbf{q}$.

Of course eqn 7.73 involves a 3-D integration, unnecessary in the case of an isotropic material where one may write [53]

$$\overline{P}(0,t) = 4\pi \int_0^\infty E(q,t)q^2 dq \tag{7.74}$$

In practice, there will be some upper limit q_{max} to the integration, so that one may define the origin only to a spatial precision on the order of q_{max}^{-1}.

For a freely diffusing particle, for which the propagator may be written $(4\pi D_0 t)^{-3/2} e^{-\mathbf{R}^2/4D_0 t}$, $P_{RTO}(t) = (4\pi D_0 t)^{-3/2}$. In a simple enclosing pore space, the rate of decay of $P_{RTO}(t)$ is slower than $t^{-3/2}$. The starting point for this analysis is the eigenmode definition of the conditional probability as $\sum_n u_n(\mathbf{r})u_n^*(\mathbf{r}')\exp(-k_n^2 t)$, from which we may write

$$\overline{P}(0,t) = \frac{1}{V_p}\sum_n |u_n(\mathbf{r})|^2 \exp(-k_n^2 t)$$
$$= \frac{1}{V_p}\sum_n \exp(-k_n^2 t) \tag{7.75}$$

the pore density being represented by $\rho(\mathbf{r}) = V_p^{-1}$. Consider the limit $t \to 0$. Just as the time-dependent diffusion coefficient, normalised by its free diffusion value D_0, may be shown to diminish at a rate proportional to both $t^{1/2}$ and the pore surface-to-volume ratio, S/V_p, so it may be shown [53] that for small t, $\overline{P}(0,t)$ normalised by its free diffusion limit $(4\pi D_0 t)^{-3/2}$ increases at this same rate. From reference [53]

$$\overline{P}(0,t)(4\pi D_0 t)^{3/2} = 1 + \frac{\sqrt{\pi}}{2}\frac{S}{V_p}\sqrt{D_0 t} + O(D_0 t) \tag{7.76}$$

While diffusion in the pore space is hindered by the reflecting surfaces, reducing the mean-square distance travelled by the particles, these same surfaces have the effect of increasing the return to origin probability. Thus the early-time behaviour of both D_{eff}, which derives from the low q limit of $E(q,t)$, and the return to origin probability, which derives from the q-integral of $E(q,t)$, provide similar insight.

At times comparable with or longer than that required to diffuse, the pore scale, $P_{RTO}(t)$, can provide additional information regarding the connectedness of a porous matrix. Schwartz *et al.* [54] have carried out both simulations and periodic lattice eigenmode calculations to show that $P_{RTO}(t)$, normalised by its free diffusion limit, rises to a maximum at a time $t \sim a^2/D_0$, declining at longer times. These authors argue that, in disordered systems, the existence of the maximum arises from pore connectedness and is controlled by the two competing effects of 'bounce back' and the trapping of diffusing particles in very small pores. While these effects are not well understood, they do have the potential to be used to complement q-space diffraction measurements and the determination of $D_{\text{eff}}(t)$ from the low-q behaviour of the echo attenuation.

References

[1] R. J. Hayward, K. J. Packer, and D. J. Tomlinson. Pulsed field-gradient spin echo N.M.R. studies of flow in fluids. *Molecular Physics*, 23:1083, 1972.

[2] P. T. Callaghan, A. Coy, D. Macgowan, K. J. Packer, and F. O. Zelaya. Diffraction-like effects in NMR diffusion studies of fluids in porous solids. *Nature*, 351:467, 1991.

[3] P. T. Callaghan. Pulsed field gradient nuclear magnetic resonance as a probe of liquid state molecular organisation. *Australian Journal of Physics*, 37:359, 1984.

[4] D. G. Cory and A. N. Garroway. Measurement of translational displacement probabilities by NMR: An indicator of compartmentation. *Magn. Reson. Med.*, 14:435, 1990.

[5] P. T. Callaghan, D. MacGowan, K. J. Packer, and F. O. Zelaya. High resolution q-space imaging in porous structures. *J. Magn. Reson*, 90:177, 1990.

[6] J. E. Tanner and E. O. Stejskal. Restricted self-diffusion of protons in colloidal systems by pulsed-gradient spin echo method. *J. Chem. Phys.*, 49:1768, 1968.

[7] D. C. Champeney. *Fourier transformations and their physical applications*. Academic Press, New York, 1973.
[8] F. B. Laun and T. A. Kuder and W. Semmler and B. Stieltjes. Determination of the defining boundary in magnetic resonance diffusion measurements. *Phys. Rev. Lett.*, 107:048102, 2011.
[9] Partha P. Mitra, Pabitra N. Sen, Lawrence M. Schwartz, and Pierre Le Doussal. Diffusion propagator as a probe of the structure of porous media. *Phys. Rev. Lett.*, 68(24):3555, 1992.
[10] J. E. M. Snaar and H. Van As. NMR self-diffusion measurements in a bounded system with loss of magnetization at the walls. *J. Magn. Reson. A*, A102:318, 1993.
[11] P. T. Callaghan. Pulsed gradient spin echo NMR for planar, cylindrical and spherical pores under conditions of wall relaxation. *J. Magn. Reson. A*, 113:53, 1995.
[12] A. Coy and P. T. Callaghan. Pulsed gradient spin echo nuclear magnetic resonance for molecules diffusing between partially reflecting rectangular barriers. *J. Chem. Phys.*, 101:4599, 1994.
[13] S. J. Gibbs. Observations of diffusive diffraction in a cylindrical pore by PFG NMR. *J. Magn. Reson*, 124:223, 1997.
[14] P. Linse and O. Söderman. The validity of the short-gradient-pulse approximation in NMR studies of restricted diffusion. Simulations of molecules diffusing between planes, in cylinders and spheres. *J. Magn. Reson. A*, 116:77, 1995.
[15] G. B. Arfken and H. J. Weber. *Mathematical Methods for Physicists*. Cambridge, New York, 2005.
[16] B. Balinov, B. Jönsson, P. Linse, and O. Söderman. The NMR self-diffusion method applied to restricted diffusion. Simulation of echo attenuation from molecules in spheres and between planes. *J. Magn. Reson. A*, 104:17, 1993.
[17] M. H. Blees. The effect of finite duration of gradient pulses on the Pulsed-Field-Gradient NMR method for studying restricted diffusion. *J. Magn. Reson. A*, 109:203, 1994.
[18] P. T. Callaghan. A simple matrix formalism for spin echo analysis of restricted diffusion under generalized gradient waveforms. *J. Magn. Reson.*, 129:74, 1997.
[19] P. P. Mitra and B. I. Halperin. The effect of finite gradient-pulse widths in pulsed gradient diffusion measurements. *J. Magn. Reson. A*, 113:94, 1995.
[20] A. Caprihan, L. Z. Wang, and E.Fukushima. A multiple-narrow-pulse approximation for restricted diffusion in a time-varying field gradient. *J. Magn. Reson.*, 118:94, 1996.
[21] D.J. Bergman and K-J. Dunn. Theory of diffusion in a porous medium with applications to pulsed field gradient NMR. *Phys. Rev. B*, 50:9153, 1994.
[22] D. J. Bergman and K-J. Dunn. Self-diffusion of nuclear spins in a porous medium with a periodic microstructure. *J. Chem. Phys.*, 102:3041, 1994.
[23] D. J. Bergman and K-J. Dunn. Self-diffusion in a periodic porous medium with interface absorption. *Phys. Rev. E.*, 51:3401, 1995.
[24] D. J. Bergman, K-J. Dunn, L. M. Schwartz, and P. P. Mitra. Self-diffusion in a periodic porous medium: a comparison of different approaches. *Phys. Rev. E.*, 51:3393, 1995.

[25] P. N. Sen, L. M. Schwartz, P. P. Mitra, and B. I. Halperin. Surface relaxation and the long time diffusion coefficient in porous media: Periodic geometries. *Phys. Rev. B*, 49:215, 1994.

[26] P. N. Sen, C. Scala, and M. H. Cohen. A self-similar model for sedimentary rocks with application to the dielectric constant of fused glass beads. *Geophysics*, 46:781, 1981.

[27] P. T. Callaghan. *Principles of Nuclear Magnetic Resonance Microscopy*. Oxford, New York, 1991.

[28] P. T. Callaghan, A. Coy, T. P. J. Halpin, D. MacGowan, K. J. Packer, and F. O. Zelaya. Diffusion in porous systems and influence of pore morphology in pulsed gradient spin echo nuclear magnetic resonance studies. *J. Chem. Phys.*, 97:651, 1991.

[29] A. Coy and P. T. Callaghan. Pulsed gradient spin echo NMR diffusive diffraction experiments on water surrounding close-packed polymer spheres. *J. Colloid Interface Sci.*, 168:373, 1994.

[30] Pang-Chih Jiang, Tsyr-Yan Yu, Wann-Cherng Perng, and Lian-Pin Hwang. Pore-to-pore hopping model for the interpretation of the pulsed gradient spin echo attenuation of water diffusion in cell suspension systems. *Biophys. J.*, 80:2493, 2001.

[31] B. Håkansson, R. Pons, and O. Söderman. Structure determination of a highly concentrated W/O emulsion using Pulsed-Field-Gradient spin-echo nuclear magnetic resonance diffusion diffractograms. *Langmuir*, 15:988, 1999.

[32] Helena Wassenius, Magnus Nyden, and Brian Vincent. NMR diffusion studies of translational properties of oil inside coreshell latex particles. *J. Colloid Interface Sci.*, 264:538, 2003.

[33] Nirbhay N. Yadav and William S. Price. Impediments to the accurate structural characterisation of a highly concentrated emulsion studied using NMR diffusion diffraction. *J. Colloid Interface Sci.*, 348:163, 2009.

[34] P. W. Kuchel, A. Coy, and P. Stilbs. NMR diffusive diffraction of water revealing alignment of erythrocytes in a magnetic field and their dimesnions and membrane transport characteristics. *Magn. Reson. Med.*, 37:637, 1997.

[35] A. M. Torres, R. J. Michniewicz, B. E. Chapman, G. A. R. Young, and P. W. Kuchel. Characterisatiuon of erythrocyte shapes and sizes by NMR diffusive diffraction of water: correlation with electron micrographs. *Magn. Reson. Imaging*, 16:423, 1998.

[36] G. H. Benga, B. E. Chapman, G. C. Cox, and P. W. Kuchel. Comparative NMR studies of diffusional water permeability of red blood cells from different species: XIV. Little penguin, eudyptula minor. *Cell Biology International*, 27:921, 2003.

[37] D. G. Regan and P. W. Kuchel. Simulations of NMR-detected diffusion in suspensions of red cells: the effects of variation in membrane permeability and observation time. *Eu. Biophys. J.*, 32:671, 2003.

[38] P. W. Kuchel, T. R. Eykyn, and D. G. Regan. Measurement of compartment size in q-space experiments: Fourier transform of the second derivative. *Magn. Reson. Med.*, 52:907, 2004.

[39] G. Pages, D. Szekely, and P. W. Kuchel. Erythrocyte-shape evolution recorded with fast-measurement NMR diffusion-diffraction. *J. Magn. Reson. Imaging*, 28: 1409, 2008.

[40] G. G Maresch, A. Grupp, M. Mehring, J. U. van Schutz, and H. C. Wolf. Direct observation of one-dimensional electron spin transport in the organic conductor (FA)2AsF6 by the electron spin echo field gradient technique. *J. Phys. (Paris)*, 46:461, 1983.

[41] R. Ruf, N. Kaplan, and E. Dormann. Restricted diffusion of the conduction electrons in quasi-one-dimensional organic conductors. *Phys. Rev. Lett.*, 74:2122, 1995.

[42] P. T. Callaghan, A. Coy, E. Dormann, R. Ruf, and N. Kaplan. Pulsed gradient spin echo ESR. *J. Magn. Reson. A*, 111:127, 1994.

[43] N. Kaplan, E. Dormann, R. Ruf, A. Coy, and P. T. Callaghan. Restricted electronmotion in a one-diemnsional organic conductor: Pulsed gradient spin echo ESR in (fluoranthene)2PF6. *Phys. Rev. B*, 52:16385, 1995.

[44] M. Conradi, A. N. Garroway, D. G. Cory, and J. Miller. Generation of short intense gradient pulses. *J. Magn. Reson.*, 94:370, 1991.

[45] J. D. Seymour and P. T. Callaghan. 'Flow-diffraction' structural characterization and measurement of hydrodynamic dispersion in porous media by PGSE NMR. *J. Magn. Reson. A*, 122:90, 1996.

[46] J. Stepisnik. Spin echo attenuation of restricted diffusion as a discord of spin phase structure. *J. Magn. Reson.*, 131:339, 1998.

[47] J. Stepisnik. Validity limits of Gaussian approximation in cumulant expansion for diffusion attenuation of spin echo. *Physica B*, 270:110, 1999.

[48] J. Stepisnik. A new view of the spin echo diffusive diffraction in porous structures. *Europhys. Lett.*, 60:453, 2002.

[49] J. Stepisnik. Averaged propagator of restricted motion from the Gaussian approximation of spin echo. *Physica B*, 344:214, 2004.

[50] B. Robertson. Spin-echo decay of spins diffusing in a bounded region. *Phys. Rev.*, 151:273, 1966.

[51] C. H. Neuman. Spin-echo of spins diffusing in a bounded medium. *J. Chem. Phys.*, 60:4508, 1974.

[52] P. W. Kuchel, A. J. Lennon, and C. Durrant. Analytical solutions and simulations for spin-echo measurements of diffusion of spins in a sphere with surface and bulk relaxation. *J. Magn. Reson. B*, 112:1, 1996.

[53] P. P. Mitra, L. L. Latour, R. L. Kleinber, and C. H. Sotak. Pulsed field gradient measurements of restricted diffusion and the return-to-origin probability. *J. Magn. Reson. A*, 114:47, 1995.

[54] L. M. Schwartz, M. D. Hürlimann, K-J. Dunn, P. P. Mitra, and D. J. Bergman. Restricted diffusion and the return to the origin probability at intermediate and long times. *Phys. Rev. E*, 55:4225, 1996.